



IMPLEMENTING MULTI-SCALE AGRICULTURAL INDICATORS EXPLOITING SENTINELS

**VEGETATION FIELD DATA AND PRODUCTION OF
GROUND-BASED MAPS:**

**“AHSPECT CAMPAIGN, SOUTH-WEST, FRANCE”
22ND – 25TH JUNE 2015**

ISSUE I1.00

EC Proposal Reference N° FP7-311766

Actual submission date : January 2016

Start date of project: 01.11.2012

Duration : 40 months

Name of lead partner for this deliverable: EOLAB



Book Captain: Fernando Camacho (EOLAB)

Contributing Authors: Consuelo Latorre (EOLAB)

Jean Louis Roujean (METEO-FRANCE)

Project co-funded by the European Commission within the Seventh Framework Program (2007-2013)		
Dissemination Level		
PU	Public	X
PP	Restricted to other programme participants (including the Commission Services)	
RE	Restricted to a group specified by the consortium (including the Commission Services)	
CO	Confidential, only for members of the consortium (including the Commission Services)	

DOCUMENT RELEASE SHEET

Book Captain:	F. Camacho	Date: 04.01.2016	Sign. 
Approval:	R. Lacaze	Date: 16.03.2016	Sign. 
Endorsement:	M. Koleva	Date:	Sign.
Distribution:	Public		

CHANGE RECORD

Issue/Revision	Date	Page(s)	Description of Change	Release
	04.01.2016	All	First Issue	I1.00

TABLE OF CONTENTS

1.	<i>Background of the Document</i>	13
1.1.	Executive Summary	13
1.2.	Portfolio	13
1.3.	Scope and Objectives	14
1.4.	Content of the Document	14
2.	<i>Introduction</i>	15
3.	<i>Study area</i>	17
3.1.	Location	17
3.2.	Description of The Test Site	18
4.	<i>Ground measurements</i>	22
4.1.	Material and Methods	22
4.1.1	Digital Hemispheric Photographs (DHP)	22
4.1.2	AccuPARLP80-Ceptometer	25
4.1.3	LI-COR LAI-2200C plant canopy analyser	26
4.2.	Spatial Sampling Scheme	27
4.3.	Ground data	30
4.3.1.	Data processing	30
4.3.2.	Content of the Ground Dataset	36
5.	<i>Evaluation of the sampling</i>	39
5.1.	Principles	39
5.2.	Evaluation Based On NDVI Values	39
5.3.	Evaluation Based On Convex Hull: Product Quality Flag.	40
6.	<i>Production of ground-based maps</i>	43
6.1.	Imagery	43
6.2.	The Transfer Function	43
6.2.1.	The regression method	43
6.2.2.	Band combination	44
6.2.3.	The selected Transfer Function	45
6.3.	The High Resolution Ground Based Maps	46
6.3.1.	Mean Values	55
7.	<i>Conclusions</i>	56

8.	<i>Acknowledgements</i>	57
9.	<i>References</i>	58
10.	<i>Annex I: Description of ESUs</i>	60

LIST OF FIGURES

Figure 1: People involved in ground measurements from EOLAB and METEO-FRANCE: Carole Planque , Fernando Camacho, Consuelo Latorre and Dominique Carrer	16
Figure 2: AHSPECT test area (South-West, France) during the first campaign (black line) and location of the sites	17
Figure 3: False color composition (RGB: SWIR – NIR - RED) of TOA Reflectance Landsat-8 scene 199/30 (23rd June, 2015) covering a study area 76 x 160 km ² of the AHSPECT campaign (South-West, France). The red square outlines the 5x5 km ² area of the different sub-sites. The Sabres sub-site is not covered by this Landsat-8 scene.	18
Figure 4: Pictures over the grassland site at Meteopole, AHSPECT campaign. 22 nd June, 2015 (South-West, France).	18
Figure 5: Landscape pictures taken over Peyrousse site during the AHSPECT campaign on 23 rd of June 2015, showing dry wheat and sunflower fields.....	19
Figure 6: Landscape pictures taken over Urgons site during the AHSPECT campaign on 23 rd of June 2015, showing corn fields around the station.	19
Figure 7: Landscape pictures taken over Sabres site during the AHSPECT campaign on 24 th of June 2015, showing corn fields at different stages and a pine forest plantation around the station.....	20
Figure 8: Normal and hemispheric pictures taken over Creon d'Armagnac site during the AHSPECT campaign on 24 th of June 2015, showing corn fields.	20
Figure 9: Landscape pictures taken over Condom site during the AHSPECT campaign on 25 th of June 2015, showing Prunus plantation, sunflower and grassland fields around the station.	21
Figure 10: Landscape pictures taken over Savenès site during the AHSPECT campaign on 25 th of June 2015, showing dry wheat, and soybean fields around the station.	21
Figure 11: AccuPAR LP80-Septometer	25
Figure 12: LAI-2200C device.	26
Figure 13: LAI-2200 optical sensor with 5 zenith angles	27
Figure 14: Distribution of the sampling units (ESUs) over the different sub-sites sampled during AHSPECT campaign 22-25 June (South-West, France). Background image Google Earth (5x5 km ²). Meteopole sub-site is not included here as only 2 ESUs (1 field) was characterized (see Figure 4).	28
Figure 15: Sampling schemes for an ESU for random (left), row (centre) or regularly planted vegetation (right).	29
Figure 16: Percentages of ESUs per land cover type collected during the AHSPECT campaign on 22 nd to 25 th June, 2015 (South-West, France).....	30
Figure 17: DHP land cover examples collected during the AHSPECT campaign on 22 nd to 25 th June, 2015 (South-West, France).	31
Figure 18: Results of the CAN-EYE processing carried out on cultivated area (Sunflower SF1 ESU6). (a) Classified images. (b) DHP images. (c) Average gap fraction and (d) the clumping factor versus view zenith angle.	31
Figure 19: Estimated LAI and LAIeff variables with DHP (y-axis) using the different CAN-EYE methods: CEV5.1, CEV6.1 and Miller's formula, as compared to the averaged value provided in the database (x-axis). For LAI, Miller's formula was not used. AHSPECT campaign during 22 nd to 25 th June, 2015 (South-West, France).....	32
Figure 20: Consistency between ground estimates. Left side: LAI vs FAPAR. Right side: FAPAR vs FCOVER. AHSPECT campaign during 22 nd to 25 th June, 2015 (South-West, France).	33
Figure 21: DHP images for ESU 56 (Prunus field), showing landscape (left), understory (middle), and overstory (right), AHSPECT campaign, Condom site, France.....	34

Figure 22: Example downward classification. Top: ESU 15 (URG_C1 field). Down: ESU 59 (CON_SF1 field). AHSPECT campaign, 2015.	34
Figure 23: Example upward classification, ESU 29 (SAB_C1). AHSPECT campaign, 2015.	35
Figure 24: Example upward classification ESU 57 (CON_P3 field). AHSPECT campaign, 2015.	35
Figure 25: Examples for clumping over sunflower SAV_SF1 fields in Savenès. Left: ESU 72. Right: ESU 71. AHSPECT campaign, 2015.	36
Figure 26: LAIeff, LAI, FAPAR and FCOVER measurements per ESU acquired during AHSPECT campaign on 22 nd to 25 th June, 2015 (South-West, France). See Annex I for identification of each ESU.	37
Figure 27: Distribution of the measured biophysical variables over the ESUs, during AHSPECT campaign on 22 nd to 25 th June, 2015 (South-West, France).	38
Figure 28: Cumulative NDVI based on ESUs (green dots) compared with Minimum and Maximum values (random sampling over the whole area). AHSPECT campaign on 22 nd to 25 th June, 2015 (South-West, France)	40
Figure 29: Convex Hull test over the 76x160 km ² overlapping (AHSPECT, Landsat-8 199/30) area: clear and dark blue correspond to the pixels belonging to the 'strict' and 'large' convex hulls. Red corresponds to the pixels for which the transfer function behaves as extrapolator. AHSPECT campaign on 22 nd to 25 th June, 2015 (South-West, France).	41
Figure 30: Convex Hull test over 5x5 km ² areas: clear and dark blue correspond to the pixels belonging to the 'strict' and 'large' convex hulls. Red corresponds to the pixels for which the transfer function is extrapolating, during the AHSPECT campaign on 22 nd to 25 th June, 2015 (South-West, France).	42
Figure 31: Test of multiple regression (TF) applied on different band combinations. Band combinations are given in abscissa (1=GREEN, 2=RED, 3=NIR and 4=SWIR). The weighted root mean square error (RMSE) is presented in red along with the cross-validation RMSE in green. The numbers indicate the number of data used for the robust regression with a weight lower than 0.7 that could be considered as outliers. AHSPECT campaign on 22 nd to 25 th June, 2015 (South-West, France).	44
Figure 32: Scatter-plots of LAIeff, LAI, FAPAR and FCOVER estimated values versus ground measurements. Full dots: Weight>0.7. Empty dots: 0<Weight<0.7. Crosses: Weight=0. AHSPECT campaign on 22 nd to 25 th June, 2015 (South-West, France). Numbers in the dots identifies the corresponding ESU. Red dots are control points not used in the empirical regression.	46
Figure 33: Ground-based LAIeff maps (76x160 km ²) retrieved during the AHSPECT campaign on 22 nd to 25 th June, 2015 (South-West, France).	47
Figure 34: Ground-based LAI maps (76x160 km ²) retrieved during the AHSPECT campaign on 22 nd to 25 th June, 2015 (South-West, France).	47
Figure 35: Ground-based FAPAR maps (76x160 km ²) retrieved during the AHSPECT campaign on 22 nd to 25 th June, 2015 (South-West, France).	48
Figure 36: Ground-based FCOVER maps (76x160 km ²) retrieved during the AHSPECT campaign on 22 nd to 25 th June, 2015 (South-West, France).	48
Figure 37: Ground-based LAIeff maps (5x5 km ²) retrieved during the AHSPECT campaign on 22 nd to 25 th June, 2015 (South-West, France).	49
Figure 38: Ground-based LAI maps (5x5 km ²) retrieved during the AHSPECT campaign on 22 nd to 25 th June, 2015 (South-West, France).	50
Figure 39: Ground-based FAPAR at 10:00 SLT maps (5x5 km ²) retrieved during the AHSPECT campaign on 22 nd to 25 th June, 2015 (South-West, France).	51
Figure 40: Ground-based FCOVER map (5x5 km ²) retrieved during the AHSPECT campaign on 22 nd to 25 th June, 2015 (South-West, France).	52
Figure 41: Scatter-plots LAI vs FAPAR ground-based maps over the AHSPECT sub-sites, 22 nd to 25 th June, 2015 (South-West, France).	53

<i>Figure 42: Scatter-plots FAPAR vs FCOVER ground-based maps over the AHSPECT sub-sites, 22nd to 25th June, 2015 (South-West, France).....</i>	<i>54</i>
-----------------------------------------------------------------------------------------------------------------------------------------------------------------------	-----------

LIST OF TABLES

Table 1: Name of the sites, location and date of the measurements collected by EOLAB.	17
Table 2: Cardinality of ESUs measurements, by Variable (LAI, FAPAR, FCOVER), by Method (DHP, LAI-2200, LP-80, visual), and by Land use during the AHSPECT campaign on 22 nd to 25 th June, 2015 (South-West, France)....	29
Table 3: The Header used to describe ESUs with the ground measurements.	36
Table 4: Percentages of convex-hull test over the study areas (5x5 km ²) during the AHSPECT campaign on 22 nd to 25 th June, 2015 (South-West, France). Convex hull values: 0= extrapolation of TF, 1= strict convex hull and 2= large convex hull.	41
Table 5: Acquisition geometry of Landsat-8 data used for retrieving high resolution maps.	43
Table 6: Transfer function applied to the whole site for LAI _{eff} , LAI, instantaneous FAPAR at 10:00 SLT and FCOVER. RW stands for weighted RMSE, whereas RC stands for cross-validation RMSE.	45
Table 7: Mean values and standard deviation (STD) of the HR biophysical maps for the selected 3 x 3 km ² areas during the AHSPECT campaign on 22 nd to 25 th June, 2015 (South-West, France).	55
Table 8: Content of the dataset.	55
Table 9: Total of ESUs collected during the AHSPECT campaign on 22 nd to 25 th June, 2015 (South-West, France). Cardinality of fields, plot label, cardinality of ESUs, label, latitude, longitude, device, land cover type and date.	60

LIST OF ACRONYMS

AHSPECT	Agriculture Health SPECTrometry
CESBIO	<i>Centre d'Etudes de la BIOSphère</i>
CEOS	Committee on Earth Observation Satellite
CEOS LPV	Land Product Validation Subgroup
DG AGRI	Directorate General for Agriculture and Rural Development
DG RELEX	Directorate General for External Relations (European Commission)
DHP	Digital Hemispheric Photographs
ECV	Essential Climate Variables
EOLAB	Earth Observation LABoratory
EU	EUropean Commission
EUFAR	EUropean Facility for Airborne Research
EUROSTATS	Directorate General of the European Commission
ESU	Elementary Sampling Unit
FAPAR	Fraction of Absorbed Photo-synthetically Active Radiation
FAO	Food and Agriculture Organization
FCOVER	Fraction of Vegetation Cover
GCOS	Global Climate Observing System
GEO-GLAM	Global Agricultural Geo- Monitoring Initiative
GIO-GL	GMES Initial Operations - Global Land (GMES)
GCOS	Global Climate Observing System
GMES	Global Monitoring for Environment and Security
GPS	Global Positioning System
IMAGINES	Implementing Multi-scale Agricultural Indicators Exploiting Sentinels
INRA	<i>Institut National de la Recherche Agronomique</i>
ITAP	<i>Instituto Técnico Agronómico Provincial – Diputación de Albacete.</i>
JECAM	Joint Experiment for Crop Assessment and Monitoring
MSG	Meteosat Second Generation satellite
LAI	Leaf Area Index
LDAS	Land Data Assimilation System
LIDAR	Laser Imaging Detection and Ranging
LUT	Look-up-table techniques
NERC- ARSF	Natural Environment Research Council - Airborne Research and Survey Facility
NPV	Non Photosynthetic Vegetation
OLIVE	On Line Validation Exercise
PAI	Plant Area Index
PAR	Photo-synthetically Active Radiation

PROBA-V	Project for On-Board Autonomy satellite, the V standing for vegetation.
RC	Cross Validated RMSE
RMSE	Root Mean Square Error
RW	Weighted RMSE
SMOS-MANIA	Soil Moisture Observing System - Meteorological Automatic Network Integrated Application
SPOT /VGT	Satellite Pour l'Observation de la Terre / VEGETATION
SCI	GMES Services Coordinated Interface
SLT	Solar Local Time
TOA	Top of Atmosphere Reflectance
USGS	U.S. Geological Survey Science organization
UTM	Universal Transverse Mercator coordinates system
VALERI	Validation of Land European Remote sensing Instruments
WGCV	Working Group on Calibration and Validation (CEOS)

1. BACKGROUND OF THE DOCUMENT

1.1. EXECUTIVE SUMMARY

The Copernicus Land Service has been built in the framework of the FP7 geoland2 project, which has set up pre-operational infrastructures. ImagineS intends to ensure the continuity of the innovation and development activities of geoland2 to support the operations of the global land component of the GMES Initial Operation (GIO) phase. In particular, the use of the future Sentinel data in an operational context will be prepared. Moreover, IMAGINES will favor the emergence of new downstream activities dedicated to the monitoring of crop and fodder production.

The main objectives of ImagineS are to (i) improve the retrieval of basic biophysical variables, mainly LAI, FAPAR and the surface albedo, identified as Terrestrial Essential Climate Variables, by merging the information coming from different sensors (PROBA-V and Landsat-8) in view to prepare the use of Sentinel missions data; (ii) develop qualified software able to process multi-sensor data at the global scale on a fully automatic basis; (iii) complement and contribute to the existing or future agricultural services by providing new data streams relying upon an original method to assess the above-ground biomass, based on the assimilation of satellite products in a Land Data Assimilation System (LDAS) in order to monitor the crop/fodder biomass production together with the carbon and water fluxes; (iv) demonstrate the added value of this contribution for a community of users acting at global, European, national, and regional scales.

Further, ImagineS will serve the growing needs of international (e.g. FAO and NGOs), European (e.g. DG AGRI, EUROSTATS, DG RELEX), and national users (e.g. national services in agro-meteorology, ministries, group of producers, traders) on accurate and reliable information for the implementation of the EU Common Agricultural Policy, of the food security policy, for early warning systems, and trading issues. ImagineS will also contribute to the Global Agricultural Geo-Monitoring Initiative (GEO-GLAM) by its original agriculture service which can monitor crop and fodder production together with the carbon and water fluxes and can provide drought indicators, and through links with JECAM (Joint Experiment for Crop Assessment and Monitoring).

1.2. PORTFOLIO

The ImagineS portfolio contains global and regional biophysical variables derived from multi-sensor satellite data, at different spatial resolutions, together with agricultural indicators, including the above-ground biomass, the carbon and water fluxes, and drought indices resulting from the assimilation of the biophysical variables in the Land Data Assimilation System (LDAS).

The production in Near Real Time of the 333m resolution products, at a frequency of 10 days, using PROBA-V data is carried out in the Copernicus Global Land Service.

The demonstration of high resolution (30m) products derived from Landsat-8 is done over demonstration sites of cropland and grassland in contrasting climatic and environmental conditions.

1.3. SCOPE AND OBJECTIVES

The main objective of this document is to describe the AHSPECT field campaign and ground data collected over multiple sites at South-West, France, and the up-scaling of the ground data to generate ground-based high resolution maps of the following biophysical variables:

- Leaf Area Index (LAI), defined as half of the total developed area of leaves per unit ground surface area (m^2/m^2). We focused on two different LAI quantities (for green elements):
 - The effective LAI (LAI_{eff}) derived from the description of the gap fraction as a function of the view zenith angle. In addition, effective LAI measures derived at 57.5° are also provided in the ground database.
 - The actual LAI (LAI) corrected from the clumping index.
- Fraction of green vegetation cover (FCover), defined as the proportion of soil covered by vegetation, derived from the gap fraction between 0 and 10° of view zenith angle.
- Fraction of Absorbed Photosynthetically Active Radiation (FAPAR), which is the fraction of the photosynthetically active radiation (PAR) absorbed by a vegetation canopy. We are also focused on green elements. PAR is the solar radiation reaching the canopy in the $0.4\text{--}0.7\ \mu\text{m}$ wavelength region. We focused on the instantaneous ‘black-sky’ FAPAR at 10:00h Solar Local Time (SLT), which is the FAPAR under direct illumination conditions at a given solar position. In addition, two other quantities are provided: daily integrated FAPAR computed as the black-sky FAPAR integrated over the day and the ‘white-sky’ FAPAR, which is the FAPAR under diffuse illumination conditions.

1.4. CONTENT OF THE DOCUMENT

This document is structured as follows:

- Chapter 2 provides an introduction to the field experiment.
- Chapter 3 provides the location and description of the site.
- Chapter 4 describes the ground measurements, including material and methods, sampling and data processing.
- Chapter 5 provides an evaluation of the sampling.
- Chapter 6 describes the production of high resolution ground-based maps, and the selected “mean” values for validation.

2. INTRODUCTION

Validation of remote sensing products is mandatory to guaranty that the satellite products meets the user's requirements. Protocols for validation of global LAI products are already developed in the context of Land Product Validation (LPV) group of the Committee on Earth Observation Satellite (CEOS) for the validation of satellite-derived land products (Fernandes et al., 2014), and recently applied to Copernicus global land products based on SPOT/SGT observations (Camacho et al., 2013). This generic approach is made of 2 major components:

- The indirect validation: including inter-comparison between products as well as evaluation of their temporal and spatial consistency
- The direct validation: comparing satellite products to ground measurements of the corresponding biophysical variables. In the case of low and medium resolution sensors, the main difficulty relies on scaling local ground measurements to the extent corresponding to pixels size. However, the direct validation is limited by the small number of sites, for that reason a main objective of ImagineS is the collection of ground truth data in demonstration sites.

The content of this document is compliant with existing validation guidelines (for direct validation) as proposed by the CEOS LPV group (Morissette et al., 2006); the VALERI project (<http://w3.avignon.inra.fr/valeri/>) and ESA campaigns (Baret and Fernandes, 2012). It therefore follows the general strategy based on a bottom up approach: it starts from the scale of the individual measurements that are aggregated over an elementary sampling unit (ESU) corresponding to a support area consistent with that of the high resolution imagery used for the up-scaling of ground data. Several ESUs are sampled over the site. Radiometric values over a decametric image are also extracted over the ESUs. This will be later used to develop empirical transfer functions for up-scaling the ESU ground measurements (e.g. Martínez et al., 2009). Finally, the high resolution ground based map will be compared with the medium resolution satellite product at the spatial support of the product.

The AHSPECT (Agriculture Health SPECTrometry) campaign is aimed at collecting hyperspectral airborne measurements over agro-forestry areas of southwest France for assessing the agricultural health, physiology and satellite products validation. The project was supported by EUFAR's transnational access programme, which facilitates and funds access to the NERC ARSF aircraft - Dornier DO228, mounted with the hyperspectral camera FENIX for visible and infrared range and the hyperspectral camera OWL for thermal infrared. A LIDAR instrument is also set up on board the aircraft. Spatial resolutions for sensors vary between 0.4 and 1.5 m, owing to low altitude flight (~1.2 km). The geo-referenced and radiometric calibrated images from the three instruments are combined.

The first phase of the campaign took place on 23rd June 2015 during which several ground-based stations maintained by CESBIO, METEO-FRANCE (SMOSMANIA) and INRA, located between Toulouse and Atlantic ocean, were overflow. High temperature and clear sky conditions were encountered during the 4-hour flight around midday. Cover types sampled concern maize and wheat crops, orchard trees, forested areas and various other

crops. A second campaign took place on 1st October 2015. It was focused on forests impacted by climate change and also vineyards.

This report presents the ground data (LAI, FAPAR and vegetation cover fraction) collected by EOLAB during the first campaign (Figure 1) and the up-scaling performed to generate ground-based maps using Landsat-8 data over several AHSPECT sites which are presented in Chapter 3.

Field Campaigns: 22nd to 25th June, 2015.

Team involved in field collection:

F. Camacho, C. Latorre (EOLAB)

Contact:

EOLAB: Fernando Camacho - fernando.camacho@eolab.es

METEOFRANCE: Jean-Louis Roujean – jean-louis.roujean@meteo.fr



**Figure 1: People involved in ground measurements from EOLAB and METEO-FRANCE:
Carole Planque , Fernando Camacho, Consuelo Latorre and Dominique Carrer**

3. STUDY AREA

3.1. LOCATION

Our measurements were taken in seven sub-sites where ground-based stations are maintained by CESBIO, METEO-FRANCE (SMOSMANIA) and INRA, located between Toulouse and Atlantic Ocean. The sites are located in the Midi-Pyrénées and Aquitania regions in the South-West of France. The several sub-sites for the first campaign are shown in Figure 2. EOLAB took ground measurements in seven (of nine) sub-sites as described in Table 1.



Figure 2: AHSPECT test area (South-West, France) during the first campaign (black line) and location of the sites

Table 1: Name of the sites, location and date of the measurements collected by EOLAB.

CAMPAIGN		Latitud	Longitude	DATES
Meteopole	MTO	43.572812° N	+1.374512° E	22 nd June 2015
Peyrouse	PEY	43.666229° N	+0.219540° E	23 th June 2015
Urgons	URG	43.639704° N	-0.433956° E	
Sabres	SAB	44.147505° N	-0.845486° E	24 th June 2015
Creón d'Armagnac	CRE	43.993601° N	-0.046897° E	
Condom	CON	43.974290° N	+0.335969° E	25 th June 2015
Savenès	SAV	43.824221° N	+1.174945° E	

Figure 3 shows a color composition of Landsat-8 image (TOA reflectance) used for up-scaling the ground values. Only 6 sub -sites fall within the Landsat-8 199/30 scene, covering an area of 76x160 km² for this date (23rd June, 2015). The available Landsat scene for Sabres sub-site corresponds to a different date, and thus it was not used for up-scaling with the other sub-sites. Finally, the ground data from Sabres was not up-scaled due to the low number of ESUs and its different canopy architecture (Pine Poplar and Corn).

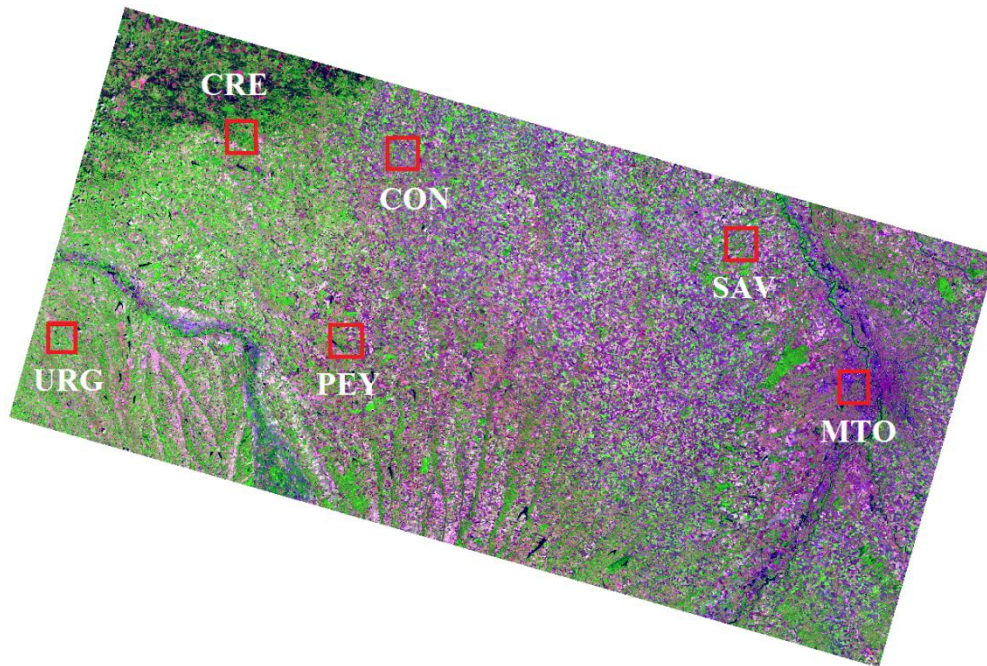


Figure 3: False color composition (RGB: SWIR – NIR - RED) of TOA Reflectance Landsat-8 scene 199/30 (23rd June, 2015) covering a study area 76 x 160 km² of the AHSPECT campaign (South-West, France). The red square outlines the 5x5 km² area of the different sub-sites. The Sabres sub-site is not covered by this Landsat-8 scene.

3.2. DESCRIPTION OF THE TEST SITE

The study region is generally flat or with small slopes with large crop fields and covered by a mix of irrigated (mainly maize and soybean) and non-irrigated crops (mainly sunflower, wheat and rapeseed). Other land cover types correspond to forest and natural vegetation, water bodies and urban areas. Figure 4 to Figure 10 show pictures over the test sites, where the flat landscape and large crop fields of wheat, sunflower, and maize can be observed.

- **Meteopole**

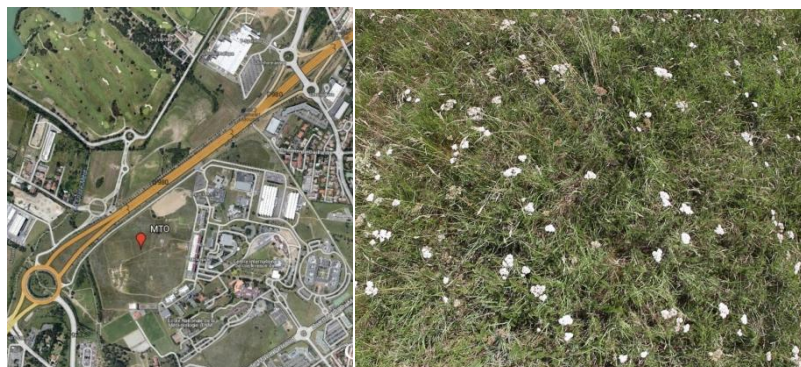


Figure 4: Pictures over the grassland site at Meteopole, AHSPECT campaign. 22nd June, 2015 (South-West, France).

- **Peyrousse**



Figure 5: Landscape pictures taken over Peyrousse site during the AHSPECT campaign on 23rd of June 2015, showing dry wheat and sunflower fields.

- **Urgons**



Figure 6: Landscape pictures taken over Urgons site during the AHSPECT campaign on 23rd of June 2015, showing corn fields around the station.

- **Sabres**



Figure 7: Landscape pictures taken over Sabres site during the AHSPECT campaign on 24th of June 2015, showing corn fields at different stages and a pine forest plantation around the station.

- **Creon d'Armagnac**



Figure 8: Normal and hemispheric pictures taken over Creon d'Armagnac site during the AHSPECT campaign on 24th of June 2015, showing corn fields.

- **Condom**



Figure 9: Landscape pictures taken over Condom site during the AHSPECT campaign on 25th of June 2015, showing Prunus plantation, sunflower and grassland fields around the station.

- **Savenès**



Figure 10: Landscape pictures taken over Savenès site during the AHSPECT campaign on 25th of June 2015, showing dry wheat, and soybean fields around the station.

4. GROUND MEASUREMENTS

The ground measurement database reported here was collected using several instruments (Section 4.1). It includes the measurements performed by EOLAB in the several sub-sites during the first phase of the AHSPECT campaign in France (Section 4.3).

4.1. MATERIAL AND METHODS

Several devices were used for estimating biophysical variables in the study area, including hemispherical digital photography (DHP), ceptometer (AccuPar LP-80) and LI-COR LAI 2200C plant canopy analyser.

4.1.1 Digital Hemispheric Photographs (DHP)

DHP were acquired with a digital camera. Hemispherical photos allow the calculation of LAI, FAPAR and FCOVER measuring gap fraction through an extreme wide-angle camera lens (i.e. 180°) (Weiss et al., 2004). It produces circular images that record the size, shape, and location of gaps, either looking upward from within a canopy or looking downward from above the canopy. The used system is composed by a professional camera and a fisheye lens: CANON EOS 6D and a SIGMA 8mm F3.5 – EX DG.

Since optical systems are not perfect, it is needed to calibrate the system in order to determinate the Optical Centre and the Projection Function (Weiss, 2010). The optical centre is defined by the projection of the optical axis onto the CCD matrix where the image is recorded. For our dual system (camera and lens), it was found in the point: (x=1378, y=896) (Latorre et al. 2014).

The hemispherical photos acquired during the field campaign were processed with the CAN-EYE software version 6.4 (developed by INRA <http://www6.paca.inra.fr/can-eye>) to derive LAI, FAPAR and FCOVER. It is based on a RGB colour classification of the image to discriminate vegetation elements from background (i.e., gaps). This approach allows exploiting downward-looking photographs for short canopies (background = soil) as well as upward-looking photographs for tall canopies (background = sky). CAN-EYE software processes simultaneously up to of 20 images acquired over the same ESU. Note that our images were acquired with similar illumination conditions to limit the variation of colour dynamics between images.

The processing is achieved in 3 main steps (Weiss et al., 2004). First, image pre-processing is performed, which includes removing undesired objects (e.g. operator, sun glint) and image contrast adjustments to ensure a better visual discrimination between vegetation elements and background. Second, an automatic classification (k-means clustering) is applied to reduce the total number of distinctive colours of the image to 324 which is sufficient to ensure accurate discrimination capacities while keeping a small enough number of colours to be easily manipulated. Finally, a default classification based on predefined colour segmentation is first proposed and then iteratively refined by the user. The allocation

of the colours to each class (vegetation elements versus background) is the most critical phase that needs to be interactive because colours depend both on illumination conditions and on canopy elements. At the end of this process a binary image, background versus vegetation elements (including both green and non-green elements) is obtained.

The CAN-EYE software computes biophysical variables from gap fraction as follows:

Effective LAI (LAI_{eff}): Among the several methods described in Weiss et al (2004), the effective LAI estimation in the CAN-EYE software is performed by model inversion. The effective LAI is estimated from the Plant Area Index (PAI) which is the variable estimated by CAN-EYE, as no distinction between leaves or other plant elements are made from the gap fraction estimates. PAI is very close to the effective LAI for croplands when pictures are taken downward looking, whereas larger discrepancies are expected for forest when pictures are taken upward looking. Effective LAI is directly retrieved by inverting Eq. (1) (Poisson model) and assuming an ellipsoidal distribution of the leaf inclination using look-up-table (LUT) techniques.

$$P_0(\theta_v, \varphi_v) = e^{-N \cdot (\theta_v, \varphi_v)} = e^{-G \cdot (\theta_v, \varphi_v) \cdot \frac{LAI_{eff}}{\cos(\theta_v)}} \quad \text{Eq. (1)}$$

A large range of random combinations of LAI (between 0 and 10, step of 0.01) and ALA (Average Leaf Angle) (10° and 80° , step of 2°) values is used to build a database made of the corresponding gap fraction values (Eq.1) in the zenithal directions defined by the CAN-EYE user (60° for the DHP collection in this field campaign). The process consists then in selecting the LUT element in the database that is the closest to the measured P_0 . The distance (cost function C_k) of the k^{th} element of the LUT to the measured gap fraction is computed as the sum of two terms. The first term computes a weighted relative root mean square error between the measured gap fraction and the LUT one. The second term is the regularization term that imposes constraints to improve the PAI estimates. Two equations are proposed for the second “regularization” term:

(1) constraint used in CAN-EYE V5.1 on the retrieved ALA values that assume an average leaf angle close to $60^\circ \pm 03^\circ$, and

(2) constraint used in CAN-EYE V6.1 on the retrieved PAI value that must be close from the one retrieved from the zenithal ring at 57° . This constraint is more efficient, but it can be computed only when the 57° ring is available (i.e., $COI \geq 60^\circ$)

The software also proposed other ways of computing PAI and ALA effective using Miller's formula (Miller, 1967) which assumed that gap fraction only depends from view zenith angle. Furthermore, the CAN-EYE makes an estimation using the Welles and Norman (1991) method used in LAI-2000 for 5 rings. These LAI2000-like estimates were not used here as are based on the same Miller's formula but using limited angular sampling.

LAI: The actual LAI that can be measured only with a planimeter with however possible allometric relationships to reduce the sampling, is related to the effective leaf area index through:

$$LAI_{eff} = \lambda_0 \cdot LAI \quad \text{Eq. (2)}$$

where λ_0 is the clumping index. In CAN-EYE, the clumping index is computed using the Lang and Xiang (1986) logarithm gap fraction averaging method, although some uncertainties are associated to this method (Demarez et al., 2008). The principle is based on the assumption that vegetation elements are locally assumed randomly distributed. Values of clumping index given by CAN_EYE are in certain cases correlated with the size of the cells used to divide photographs. The values reported here were estimated with an average of the three results (CEV6.1, CEV5.1 and Miller).

As the CAN-EYE software provides different results (CEV6.1, CEV5.1 and Miller's) for LAI_{eff} and LAI variables; an average LAI value was provided as ground estimate, and the standard deviation of the different method LAI estimates was reported as the uncertainty of the estimate (see associated 2015_VGM_AHSPECT.xls file). Note that for LAI, only CEV6.1 and CEV5.1 were used.

FCOVER is retrieved from gap fraction between 0 to 10°.

$$FCOVER = 1 - P_0 \cdot (0 - 10^\circ) \quad \text{Eq. (3)}$$

FAPAR: As there is little scattering by leaves in that particular spectral domain due to the strong absorbing features of the photosynthetic pigments, FAPAR is often assumed to be equal to FIPAR (Fraction of Intercepted Photosynthetically Active Radiation), and therefore directly related to the gap fraction. The actual FAPAR is the sum of two terms, weighted by the diffuse fraction in the PAR domain: the 'black sky' FAPAR that corresponds to the direct component and the 'white sky' or the diffuse component.

The instantaneous "Black-sky FAPAR" ($FAPAR^{BS}$) is given at a solar position (date, hour and latitude). Depending on latitude, the CAN EYE software computes the solar zenith angle every solar hour during half the day (there is symmetry at 12:00). The instantaneous FAPAR is then approximated at each solar hour as 1 minus the gap fraction in the corresponding solar zenith angle:

$$FAPAR^{BS}(\theta_s) = 1 - P_0 \cdot (\theta_s) \quad \text{Eq. (4)}$$

The "daily integrated" black-sky FAPAR is computed as the following:

$$FAPAR_{Day}^{BS} = \frac{\int_{sunset}^{sunrise} \cos(\theta_s) \cdot [1 - P_0(\theta_s)] \cdot d\theta}{\int_{sunset}^{sunrise} \cos(\theta_s) \cdot d\theta} \quad \text{Eq. (5)}$$

The “white-sky (or diffuse) FAPAR” is computed as the following:

$$FAPAR^{ws} = \frac{1}{\pi} \int_0^{2\pi} \int_0^{\pi} P_0 \cos(\theta_s) \sin(\theta_s) d\theta d\phi = 2 \cdot \int_0^{\pi} P_0 \cos(\theta_s) \sin(\theta_s) d\theta \quad \text{Eq. (6)}$$

The CAN-EYE software provides the three FAPAR variables. Instantaneous black-sky FAPAR values at 10:00h SLT were up-scaled.

4.1.2 AccuPARLP80-Ceptometer

The AccuPAR model LP-80 (Figure 11) is a lightweight, portable, linear Photosynthetically Active Radiation (PAR) sensor (Decagon Devices, Inc. 2014). It lets you measure canopy PAR interception and calculate leaf area index (LAI) at any location within a plant or forest canopy. PAR data can be used with other climate data to estimate biomass production without destroying the crop. PAR is also important in determining other canopy processes; such as radiation interception, energy conversion, momentum, gas exchange, precipitation interception, and evapotranspiration.

It consists of an integrated microprocessor-driven data logger and probe. The probe contains 80 independent sensors, spaced 1 cm apart. The photo sensors measure PAR in the 400 to 700 nm waveband. The AccuPAR displays PAR in units of micro-mols per meter squared per second ($\mu\text{mol} \times \text{m}^{-2} \times \text{s}^{-1}$). The instrument is capable of hand-held or unattended measurement.



Figure 11: AccuPAR LP80-Ceptometer

For AccuPAR, the effective PAI is derived following the equations to predict the scattered and transmitted PAR (Norman and Welles, 1983).

$$PAI_{eff} = \frac{\left[\left(1 - \frac{1}{2k} \right) f_b - 1 \right] \ln \tau}{A(1 - 0.47f_b)} \quad \text{Eq.(7)}$$

Where τ is the transmission coefficient obtained through the ratio of the below canopy and the above canopy PARs, f_b is the fraction of incident beam PAR, A is a function of the leaf absorptivity (a) in the PAR band (AccuPAR assumes $a = 0.9$, and $A=0.86$ in LAI sampling routines), and k is the extinction coefficient for the canopy. K coefficients for typical crops are provided in the manual. It can be estimated as the ration between the height and the width of the plant. We have used a range of K values between 0.8 and 1.4 depending on the type and status of the canopy.

4.1.3 LI-COR LAI-2200C plant canopy analyser

The LAI-2200C (LI-COR Inc., Lincoln, Nebraska, 2013) is a model of plant canopy analyser used in the field campaign (Figure 12).



Figure 12: LAI-2200C device.

These instruments calculate Leaf Area Index (LAI) and other canopy attributes from light measurements made with a “fish-eye” optical sensor (148° field-of-view). Measurements made above and below the canopy are used to calculate canopy light interception at five zenith angles (Figure 13). The average probability of light penetration into the canopy is computed by

$$\overline{P(\theta_i)} = \frac{1}{N_{obs}} \sum_{j=1}^{N_{obs}} \frac{B_{ij}}{A_{ij}} \quad \text{Eq. (8)}$$

where the subscript i ($i = 1 \dots 5$) refers to the optical sensor rings centered at θ_i and j refers to the number of observational pairs ($j = 1 \dots N_{obs}$). B_{ij} and A_{ij} are the j^{th} below and above canopy readings, respectively, for the i^{th} ring. The gap fraction for the i^{th} ring is computed from

$$G_i = e^{\left(\overline{\ln P(\theta_i)}\right)} = e^{\left(\frac{1}{N_{obs}} \sum_{j=1}^{N_{obs}} \ln \frac{B_{ij}}{A_{ij}}\right)} \quad \text{Eq. (9)}$$

Assuming the foliage elements are randomly distributed in space, the effective PAI (PAI_{eff}) can be estimated by the transmittance in the different view angles based on Miller's formula (Miller, 1967).

$$PAI_{eff} = 2 \int_0^{\pi/2} -\ln P(\theta) \cos \theta \sin \theta d\theta \quad \text{Eq. (10)}$$

The amount of foliage in a vegetative canopy can be deduced from measurements of how quickly radiation is attenuated as it passes through the canopy. By measuring this attenuation at several angles from the zenith, foliage orientation information can also be obtained. The LAI-2200 measures the attenuation of diffuse sky radiation at five zenith angles simultaneously, arranged in concentric rings.

A normal measurement with the LAI-2200 consists of a minimum of ten numbers: five of the numbers are the signals from the five detectors when the optical sensor was above the vegetation, and the remaining five are the readings made with the sensor below the vegetation. For both readings, the sensor is looking up at the sky. Five values of canopy transmittance are calculated from these readings by dividing corresponding pairs.

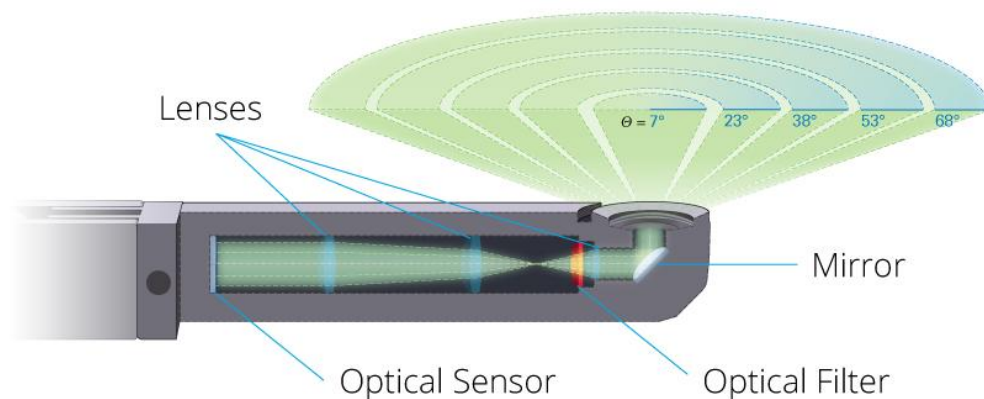


Figure 13: LAI-2200 optical sensor with 5 zenith angles

4.2. SPATIAL SAMPLING SCHEME

Based on previous experiments (e.g., VALERI project) a protocol for sampling the site and the Elementary Sampling Unit (ESU) has been designed, and proposed for running field campaigns within the FP7 ImagineS project (Camacho et al., 2015). For each site, the most representative fields around the station were characterized (see sampling in Figure 14). The fields were selected to sample the range of vegetation types and conditions encountered in the South-West zone. The location of the ESUs was recorded using a GPS that provides an accuracy of few meters.

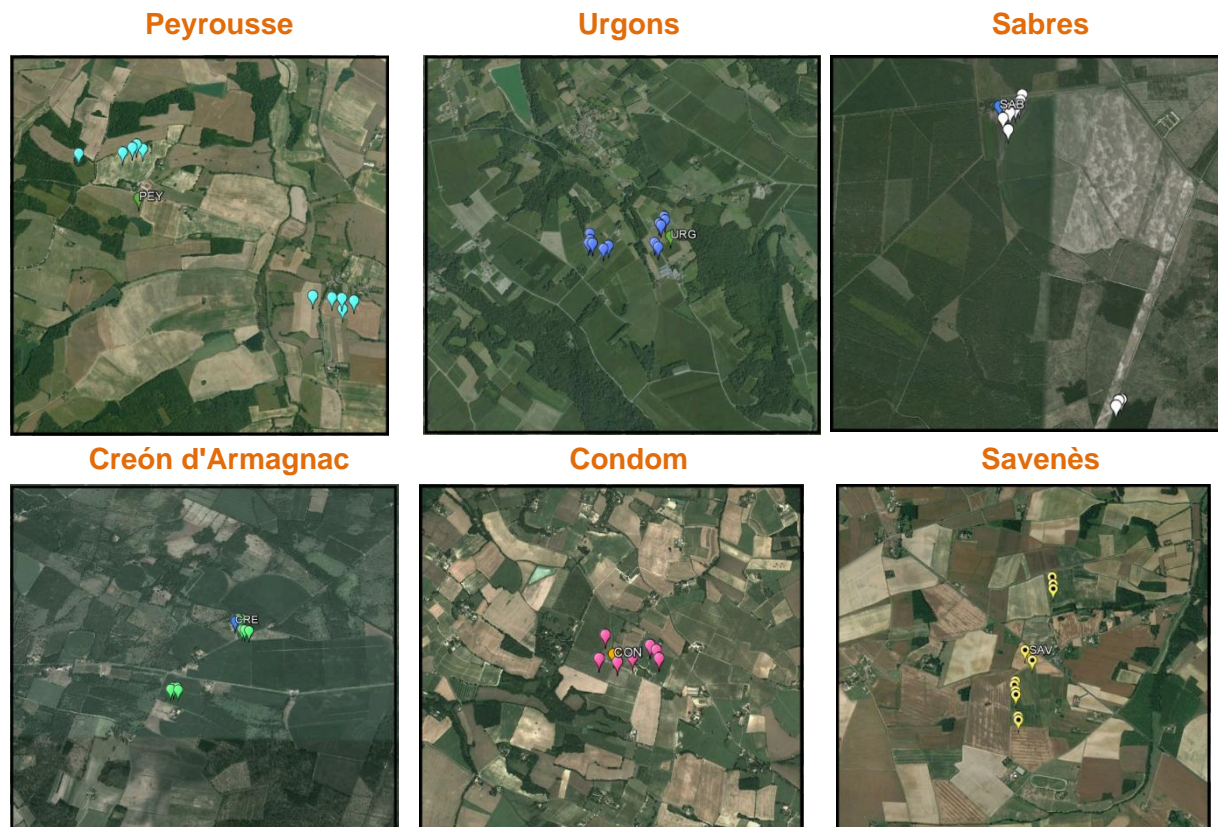


Figure 14: Distribution of the sampling units (ESUs) over the different sub-sites sampled during AHSPECT campaign 22-25 June (South-West, France). Background image Google Earth (5x5 km²). Meteopole sub-site is not included here as only 2 ESUs (1 field) was characterized (see Figure 4).

Within each field, at least 3 ESUs were measured (except for dry fields) to account for the intra-field variability. A pseudo-regular sampling was used in most of the ESUs of approximately 20x20 m² which was different depending on the spatial distribution of the plant canopy (Figure 15). Most of the ESUs were sampled following the scheme shown in Figure 15-left, whereas for Corn (row plantation) we followed the scheme of Figure 15-center. Finally, for some tree plantation (Prunus), we follow the scheme of Figure 15-right.

Within each ESU the number of DHP taken ranged between 12 and 15. For LAI-2200 and AccuPAR, we performed 27 replications (3 up x 9 down) within the ESU following the same spatial scheme, but with duplication of replications.

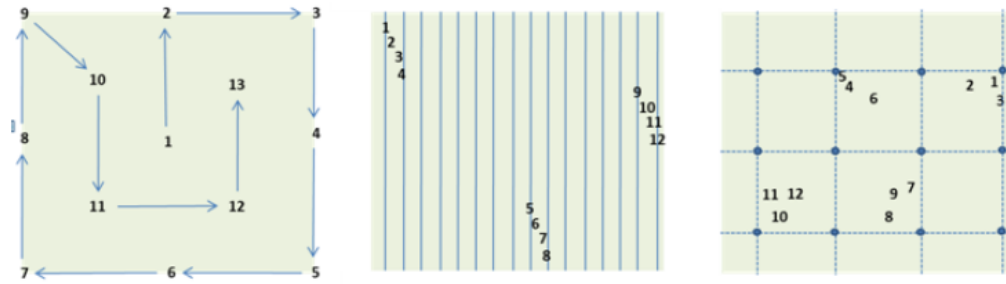


Figure 15: Sampling schemes for an ESU for random (left), row (centre) or regularly planted vegetation (right).

Finally, a total of 73 ESUs in 32 fields were characterized during the field campaign over the seven sites (see Table 2). Furthermore, additional bare areas ESUs were included in order to extend the sampling over non vegetated areas.

Table 2: Cardinality of ESUs measurements, by Variable (LAI, FAPAR, FCOVER), by Method (DHP, LAI-2200, LP-80, visual), and by Land use during the AHSPECT campaign on 22nd to 25th June, 2015 (South-West, France).

South-West sites AHSPECT		Number of ESUs by Variable				Number of measurements				
		LAI _{eff}	LAI	FAPAR	FCOVER					
Meteopole	MTO	2	2	2	2	2				
Peyrousse	PEY	12	12	12	12	12				
Urgons	URG	12	7	7	7	12				
Sabres	SAB	16	6	11	6	16				
Creón	CRE	14	8	9	8	14				
Condom	CON	8	8	8	8	8				
Savenès	SAV	13	10	10	10	13				
Total measurements		77	53	59	53	77				
AHSPECT		Number of ESUs by Method				Number of measurements				
		DHP	LAI2200	LP80	visual inspection					
Meteopole	MTO	2	-	-	-	2				
Peyrousse	PEY	11	-	-	1	12				
Urgons	URG	7	5	-	-	12				
Sabres	SAB	6	5	5	-	16				
Creón	CRE	6	5	1	2	14				
Condom	CON	8	-	-	-	8				
Savenès	SAV	9	3	-	1	13				
Total measurements		49	18	6	4	77				
AHSPECT		Number of ESUs by Land use								Number of Fields
		Wheat	Corn	Grassland	Sunflower	Harvested	PinePoplar	Prunus	Soybean	
Meteopole	MTO	-	-	2	-	-	-	-	-	1
Peyrousse	PEY	3	-	-	9	-	-	-	-	6
Urgons	URG	-	12	-	-	-	-	-	-	4
Sabres	SAB	-	9	-	-	-	7	-	-	3
Creón	CRE	-	12	1	-	1	-	-	-	5
Condom	CON	1	-	1	3	-	-	3	-	6
Savenès	SAV	3	-	-	3	1	-	-	6	7
Total measurements		7	33	4	15	2	7	3	6	32 fields
Total ESUs		73 ESUs								

AHSPECT campaign, South-West (FRANCE) June 2015

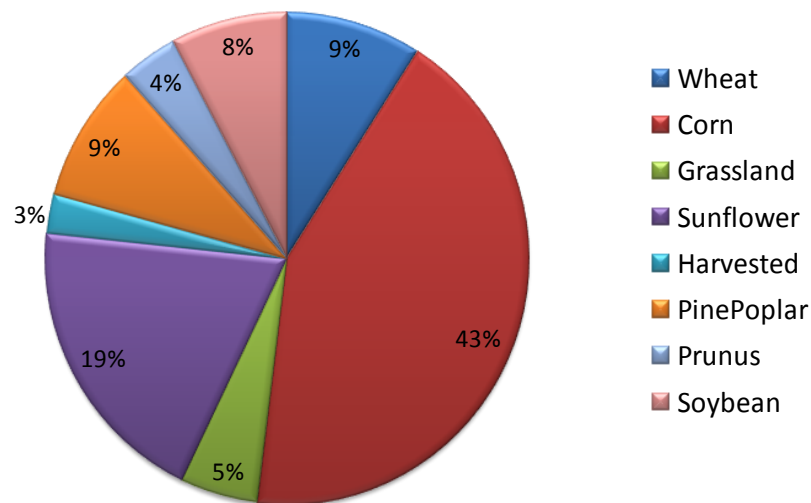


Figure 16: Percentages of ESUs per land cover type collected during the AHSPECT campaign on 22nd to 25th June, 2015 (South-West, France).

4.3. GROUND DATA

4.3.1. Data processing

The software CAN-EYE version V6.4 was used to process the DHP images. Figure 17 shows examples of DHPs. Different land cover types have been selected: wheat, prunus, pines, corn at different stages, soybean, sunflower and grassland fields. Figure 18 shows an example of the processing with the CAN-EYE, including the classification, the average gap fraction and the clumping index variation as a function of the view zenith angle.

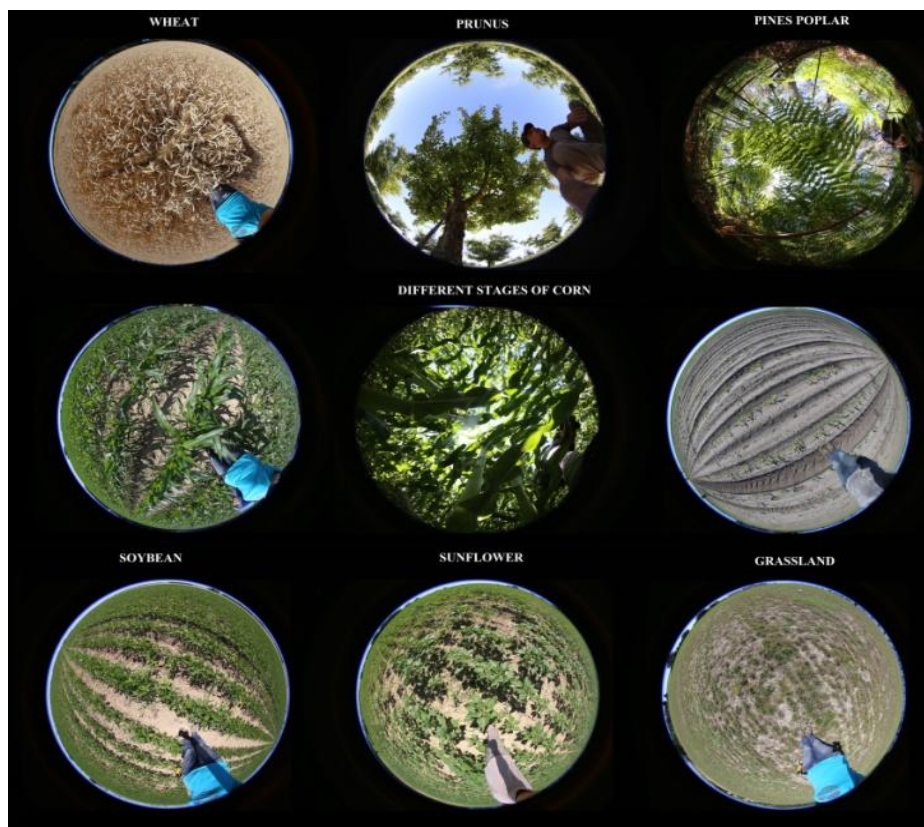


Figure 17: DHP land cover examples collected during the AHSPECT campaign on 22nd to 25th June, 2015 (South-West, France).

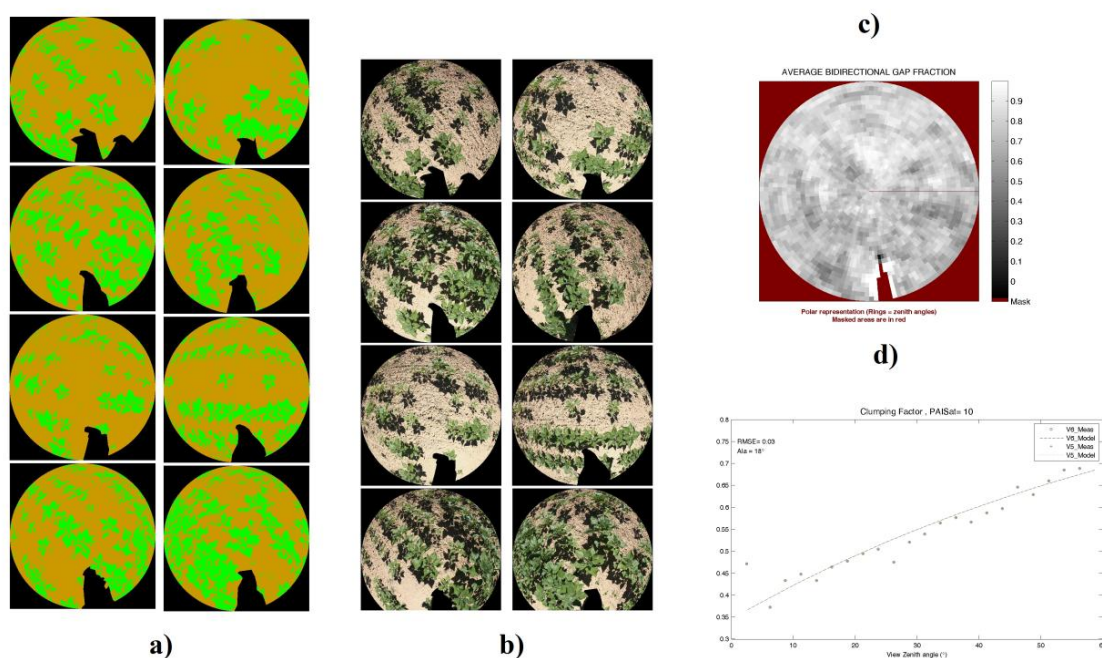


Figure 18: Results of the CAN-EYE processing carried out on cultivated area (Sunflower SF1 ESU6). (a) Classified images. (b) DHP images. (c) Average gap fraction and (d) the clumping factor versus view zenith angle.

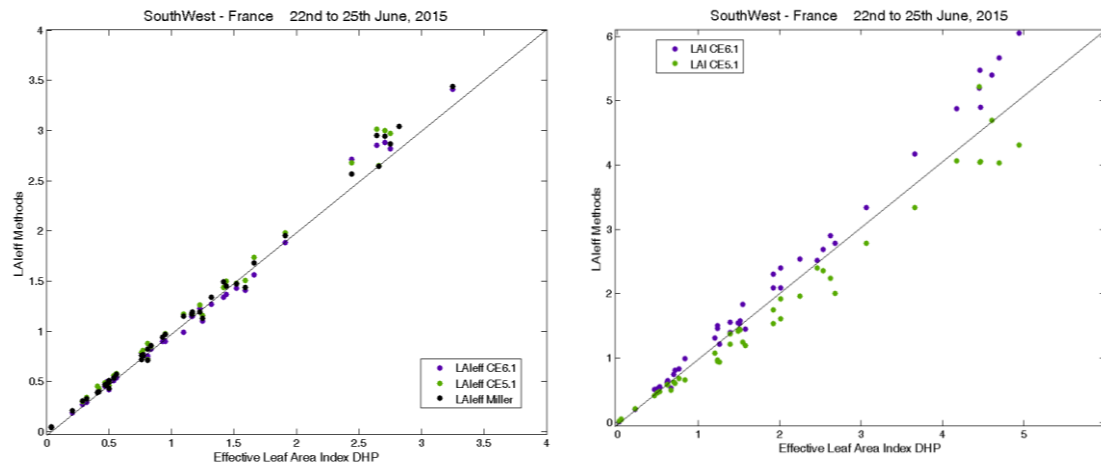


Figure 19: Estimated LAI and LAIeff variables with DHP (y-axis) using the different CAN-EYE methods: CEV5.1, CEV6.1 and Miller's formula, as compared to the averaged value provided in the database (x-axis). For LAI, Miller's formula was not used. AHSPECT campaign during 22nd to 25th June, 2015 (South-West, France).

As described at section 4.1, the LAI and effective LAI values are estimated from DHP using different methods (CEV6.1, CEV5.1 and Miller's). Figure 19 shows an inter-comparison between the three methods for LAIeff and between CEV6.1 and CEV5.1 for LAI, the averaged value provided in the database is shown in the x-axis. For LAI, we are not using Miller's formula for clumping as it is limited in the view zenith angles and the results depart notably from the two CAN-EYE methods (using all the zenith angles). For LAIeff, the results are very similar for the three methods but, for LAI, there is some dispersion between both methods, which indirectly indicates the uncertainties attached to the clumping index estimated with CAN-EYE. As an example, for the averaged LAI value close to 5, the difference between CEV6.1 and CEV5.1 is about 2 LAI units. CEV5.1 provides systematically lower LAI values than CEV6.1.

Figure 20 shows the consistency between estimated ground parameters. LAI and black-sky FAPAR at 10:00 SLT shows the typical positive exponential curve, whereas FCOVER and FAPAR shows a linear trend, with slightly higher FAPAR values as expected. Some points where the differences between FAPAR and FCOVER were found higher than 0.20 have been marked as suspicious in the ground dataset (as probably the FCOVER could be underestimated due to the sampling of the ESU with the small FOV used to estimate FCOVER with DHP). In particular, ESU#20 and ESU#42 were marked, both corresponding to Corn crops.

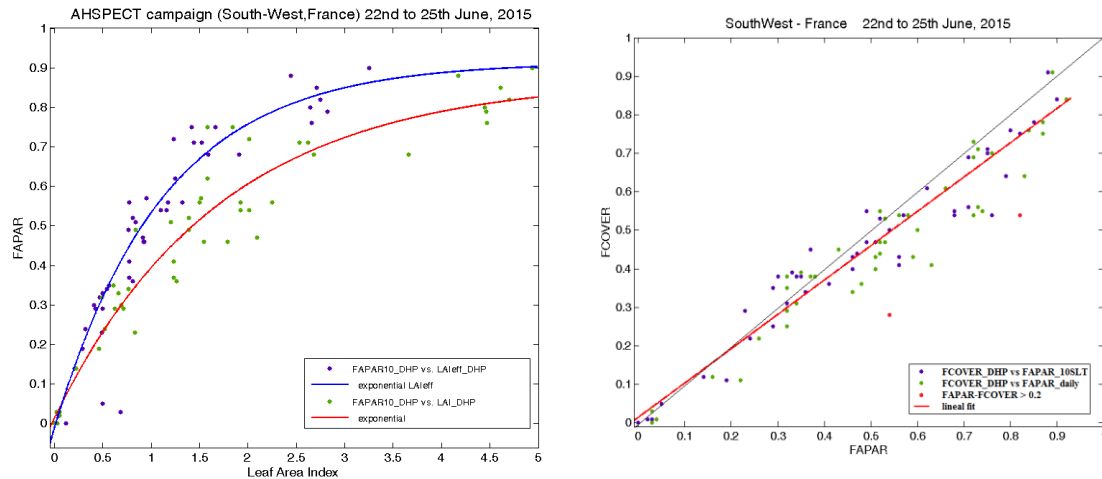


Figure 20: Consistency between ground estimates. Left side: LAI vs FAPAR. Right side: FAPAR vs FCOVER. AHSPECT campaign during 22nd to 25th June, 2015 (South-West, France).

4.3.1.1. Special cases

- **ESUs with understory and overstory**

For several ESUs (54, 56 and 58) with understory and overstory, hemispherical images were acquired upward looking (overstory) and downward looking (understory) (Figure 21). The two sets of acquisitions were processed separately to derived LAI (effective and actual), FCOVER and FAPAR. To compute FCOVER and FAPAR, the independency of the gaps inside the understory and the gaps inside the trees has been assumed. The ESU biophysical variable was then computed as:

- LAI :

$$LAI = LAI_{ABOVE} + LAI_{BELOW}$$

- FCOVER / FAPAR :

$$FCOVER = 1 - (1 - FCOVER_{ABOVE})(1 - FCOVER_{BELOW})$$

$$FAPAR = 1 - (1 - FAPAR_{ABOVE})(1 - FAPAR_{BELOW})$$



Figure 21: DHP images for ESU 56 (Prunus field), showing landscape (left), understory (middle), and overstory (right), AHSPECT campaign, Condom site, France.

- **ESUs showing non-stable CAN-EYE retrievals**

For some ESUs, some difficulties during the CAN-EYE processing were encountered depending on the classification of the image, which is a subjective process where the operator selects training areas of the main components. This happens mainly in those ESUs with shining areas in the leaves (similar to soil) and shadows over vegetation (similar to shaded background). Figure 22-top shows a corn crop where bright areas in the leaf are observed, these areas are misclassified as soils (see red arrows). If we select this bright leaves as vegetation, thus soil is misclassified as vegetation. Figure 22-bottom shows an example where shaded vegetation is misclassified as soil. This problem is very difficult to solve, as if we select shaded leaves as vegetation, then the shaded background is misclassified as vegetation.

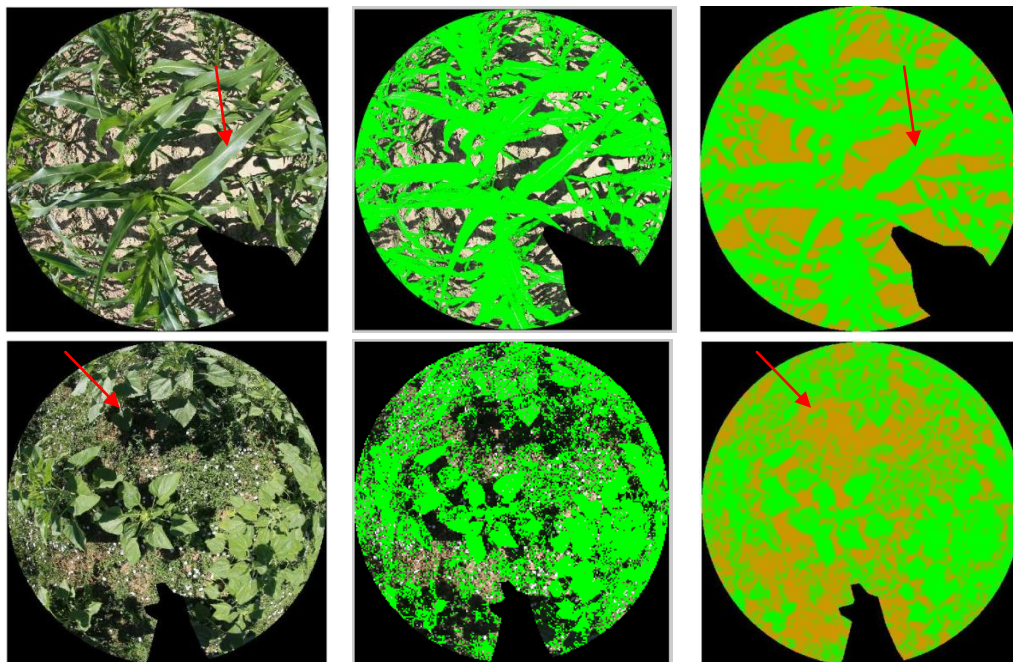


Figure 22: Example downward classification. Top: ESU 15 (URG_C1 field). Down: ESU 59 (CON_SF1 field). AHSPECT campaign, 2015.

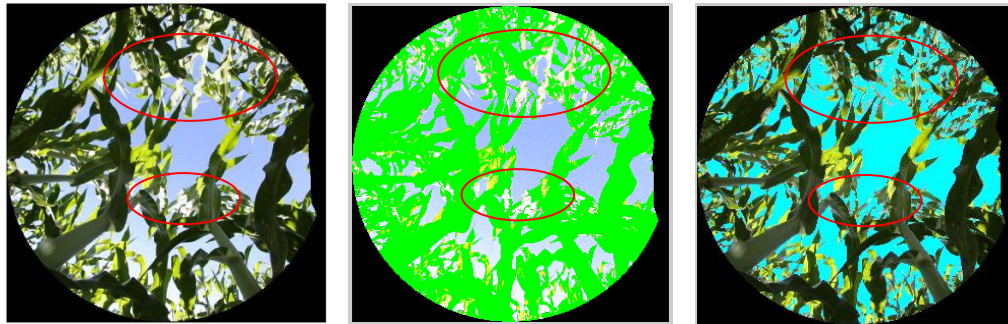


Figure 23: Example upward classification, ESU 29 (SAB_C1). AHSPECT campaign, 2015.

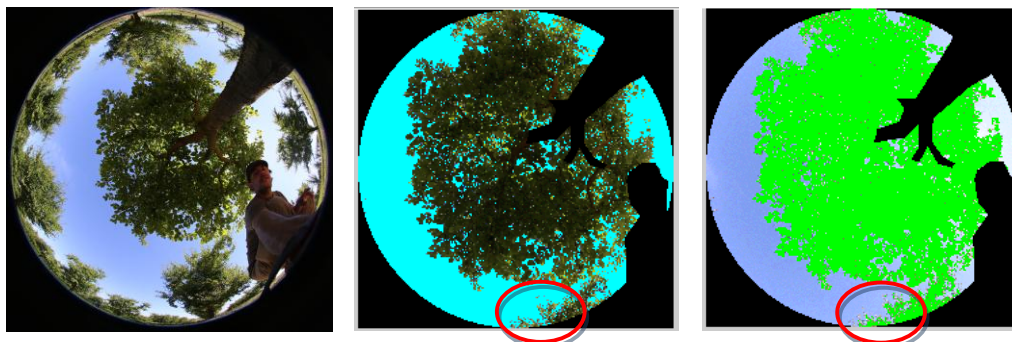


Figure 24: Example upward classification ESU 57 (CON_P3 field). AHSPECT campaign, 2015.

For upward looking photos, the processing with CAN-EYE was also sensible to the main component selected for the classification (i.e., sky or vegetation). Figure 23 and Figure 24 shows two examples of upward looking DHP processing. In Figure 23, if we select “vegetation” for performing the classification, the bright leaves are not considered, and then the green gap fraction is underestimated. On the contrary, if we select the “sky” for the classification, the vegetation is overestimated. This effect can be also observed in Figure 24.

To reduce the uncertainties of the estimate associated to the classification, we have processed these problematic ESUs twice (one classifying vegetation and other classifying sky/soil). The measured result provided in the database corresponds to the average value of the two processing. The largest uncertainty was reported.

- **ESUs with non reliable clumping**

For some ESUs, we have detected a much lower estimated clumping index than expected for an homogenous crop canopy. For instance, Figure 25 shows a pair of examples of clumping index derived from CAN-EYE for sunflower field (SAV_SF1) in Savenès. Note that the clumping index ranges between 0.74 and 0.52. These clumping index values will increase artificially the retrieved LAI up to twice the effective LAI (for ESU71). This was considered unreliable as there were only few leaves and regular distributions of plants. Some spatial heterogeneity is observed in ESU71, but the application of these clumping values

would clearly result in unreliable actual LAI. For these few cases, the clumping index value was modified and set to 0.9 in the database.

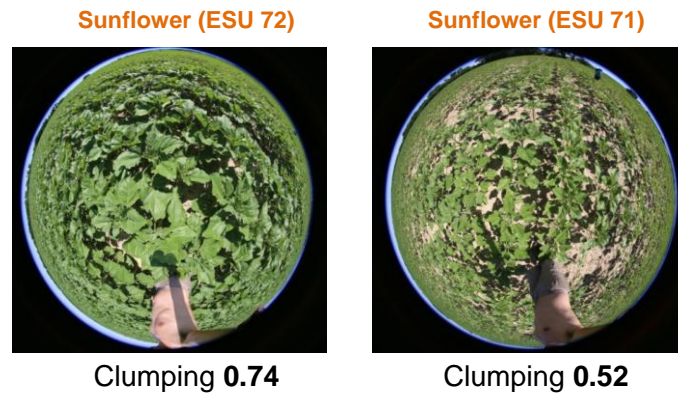


Figure 25: Examples for clumping over sunflower SAV_SF1 fields in Savenès. Left: ESU 72. Right: ESU 71. AHSPECT campaign, 2015.

4.3.2. Content of the Ground Dataset

The ground dataset is provided in an excel file (**2015_VGM_AHSPECT.xls** file). Each ESU is described according to a standard format, specifying the site name, location, and values. The header of the database is shown in Table 3.

Table 3: The Header used to describe ESUs with the ground measurements.

Column	Var.Name	Comment
1	Plot #	Number of the field plot in the site
2	Plot Label	Label of the plot in the site
3	ESU #	Number of the Elementary Sampling Unit (ESU)
4	ESU Label	Label of the ESU in the campaign
5	Northing Coord.	Geographical coordinate: Latitude (°), WGS-84
6	Easting Coord.	Geographical coordinate: Longitude (°), WGS-84
7	Extent (m) of ESU (diameter)	Size of the ESU ⁽¹⁾
8	Land Cover	Detailed land cover
9	Start Date (dd/mm/yyyy)	Starting date of measurements
10	End Date (dd/mm/yyyy)	Ending date of measurements
11	Products*	Method
12		Nb. Replications
13		PRODUCT
14		Uncertainty

*LAI_{eff}, LAI, FAPAR and FCOVER

Figure 26 shows the obtained ground values for each ESU. The identification (Plot, Site, land cover, lat, long) of each ESU is provided in Annex I. Very low values were obtained for early corn crops (ESU 33, ESU34), or bare areas or non photosynthetic vegetation (NPV) vegetation (e.g. ESU 69, ESU 70). Other crops such as Soybean (ESU 63-68) presented low values ranging between 0.5 and 1 for LAI, and around 0.3-0.4 for FCOVER/FAPAR. The highest values were found for Corn plots at Cre on d'Armagnac (ESU 39-46) with LAI up to 5, and FAPAR values ranging between 0.8 and 0.9. Intermediate values were found for other corn canopies, and sunflower fields. Over some fields (and also for some ESUs) different devices were used, DHP, LAI2200 and LP80, all of them provided consistent LAIeff values, with differences typically lower than 0.5 units, see for instance ESU#17-ESU#20 or ESU#21-ESU#24 (Corn fields) measured with LAI-2000 and DHP, or ESU#36 (Pine poplar) measured with the three devices. The exception was ESU#43 where LAI2200 provided significant higher values than DHP or LP-80, and ESU#29 where DHP and LP-80 provided quite different estimates. The comparison of FAPAR between AccuPAR and DHP were found also consistent (e.g., ESU#29 or ESU#36).



Figure 26: LAIeff, LAI, FAPAR and FCOVER measurements per ESU acquired during AHSPECT campaign on 22nd to 25th June, 2015 (South-West, France). See Annex I for identification of each ESU.

The distribution of the measured variables is presented in Figure 27. A good distribution of values covering almost the whole dynamic range is obtained. The exceptions were only very high vegetation values that were under-sampled. Distributions of LAI values range mostly between 0 and 2, with some values around 4.5. For FAPAR the larger distribution of values is between 0.7 and 0.8, and for FCOVER between 0.4 and 0.6.

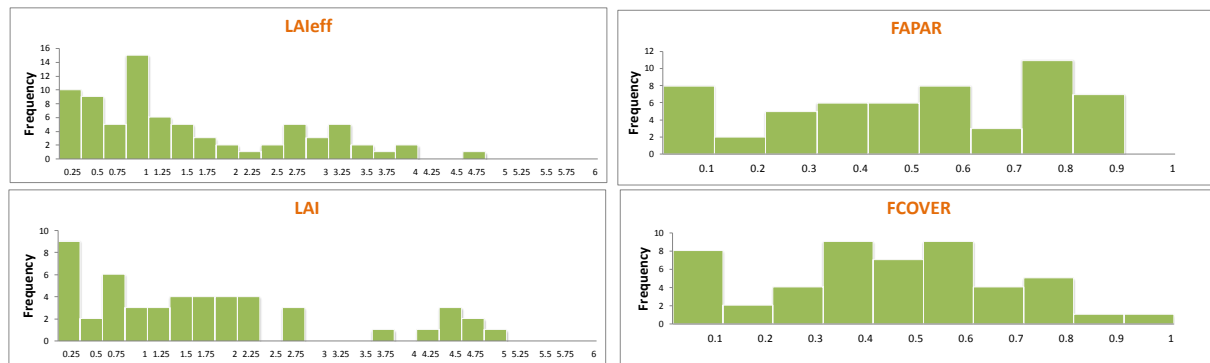


Figure 27: Distribution of the measured biophysical variables over the ESUs, during AHSPECT campaign on 22nd to 25th June, 2015 (South-West, France).

5. EVALUATION OF THE SAMPLING

5.1. PRINCIPLES

Based on the experience gained in previous field activities, the data set sampling was concentrated in the most representative areas. The number of sampling points (including ESUs, ESU control points (ECP) and ground control points (GCP)) was 73 ESUs. 16 ESUs belongs to Sabres sub-site outside of the Landsat scene, therefore only 57 were used for up-scaling; the several ECPs have been used to verify the empirical retrievals over bare and senescent areas.

5.2. EVALUATION BASED ON NDVI VALUES

The sampling strategy is evaluated using the Landsat-8 image by comparing the NDVI distribution over the site with the NDVI distribution over the ESUs (Figure 28). As the number of pixels is drastically different for the ESU and whole site (WS), it is not statistically consistent to directly compare the two NDVI histograms. Therefore, the proposed technique consists in comparing the NDVI cumulative frequency of the two distributions by a Monte-Carlo procedure which aims at comparing the actual frequency to randomly shifted sampling patterns. It consists in:

1. computing the cumulative frequency of the N pixel NDVI that correspond to the exact ESU locations; then, applying a unique random translation to the sampling design (modulo the size of the image)
2. computing the cumulative frequency of NDVI on the randomly shifted sampling design
3. repeating steps 1 and 2, 199 times with 199 different random translation vectors.

This provides a total population of $N = 199 + 1$ (actual) cumulative frequency on which a statistical test at acceptance probability $1 - \alpha = 95\%$ is applied: for a given NDVI level, if the actual ESU density function is between two limits defined by the $N\alpha/2 = 5$ highest and lowest values of the 200 cumulative frequencies, the hypothesis assuming that WS and ESU NDVI distributions are equivalent is accepted, otherwise it is rejected.

Figure 28 shows the TOA NDVI distribution during the AHSPECT campaign on 22nd to 25th June, 2015 (South-West, France). As can be observed the spatial sampling does not present bias toward high or low vegetation values. The convex hull map will provide further information on the representativeness of the spatial sampling (Section 5.3).

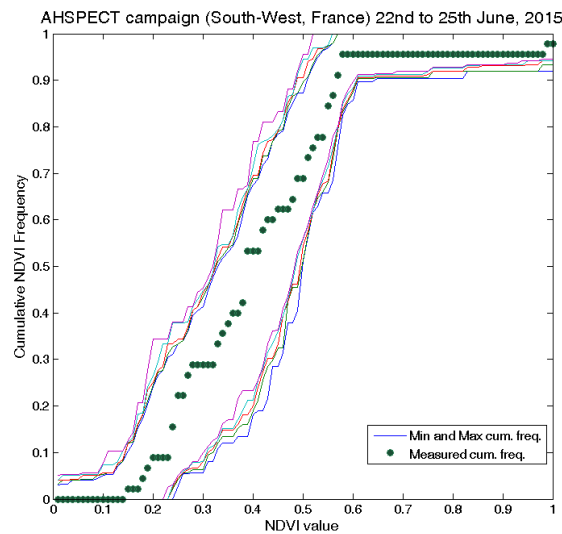


Figure 28: Cumulative NDVI based on ESUs (green dots) compared with Minimum and Maximum values (random sampling over the whole area). AHSPECT campaign on 22nd to 25th June, 2015 (South-West, France)

5.3. EVALUATION BASED ON CONVEX HULL: PRODUCT QUALITY FLAG.

The interpolation capabilities of the empirical transfer function used for up-scaling the ground data using decametric images is dependent of the sampling (Martinez et al., 2009). A test based on the convex hulls was also carried out to characterize the representativeness of ESUs and the reliability of the empirical transfer function using the different combinations of the selected bands (green, red, NIR and SWIR) of the Landsat-8 image. A flag image is computed over the reflectances. The result on convex-hulls can be interpreted as:

- pixels inside the 'strict convex-hull': a convex-hull is computed using all the Landsat-8 reflectances corresponding to the ESUs belonging to the class. These pixels are well represented by the ground sampling and therefore, when applying a transfer function the degree of confidence in the results will be quite high, since the transfer function will be used as an interpolator;
- pixels inside the 'large convex-hull': a convex-hull is computed using all the reflectance combinations ($\pm 5\%$ in relative value) corresponding to the ESUs. For these pixels, the degree of confidence in the obtained results will be quite good, since the transfer function is used as an extrapolator (but not far from interpolator);
- pixels outside the two convex-hulls: this means that for these pixels, the transfer function will behave as an extrapolator which makes the results less reliable. However, having a priori information on the site may help to evaluate the extrapolation capacities of the transfer function.

Figure 29 shows the results of the Convex-Hull test (i.e., Quality Flag image) for the AHSPECT campaign on 22nd to 25th June, 2015 (South-West, France) over the AHSPECT area covered by the selected Landsat-8 scene.

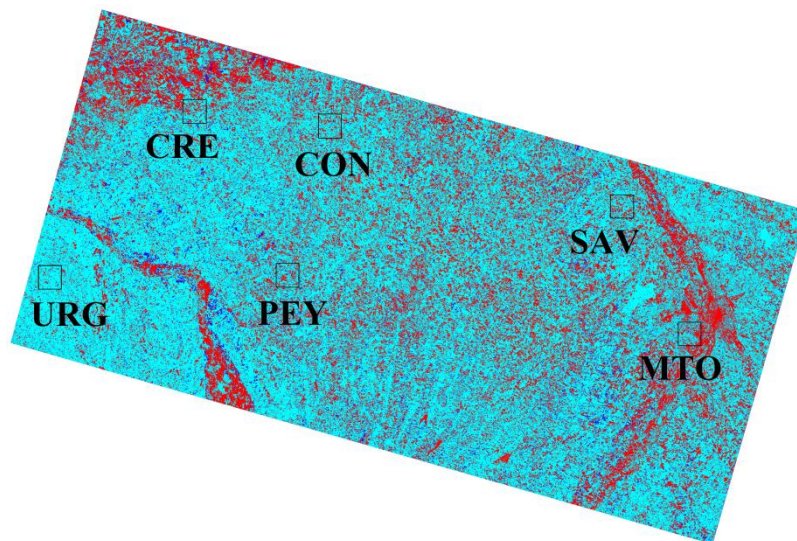


Figure 29: Convex Hull test over the 76x160 km² overlapping (AHSPECT, Landsat-8 199/30) area: clear and dark blue correspond to the pixels belonging to the 'strict' and 'large' convex hulls. Red corresponds to the pixels for which the transfer function behaves as extrapolator. AHSPECT campaign on 22nd to 25th June, 2015 (South-West, France).

Figure 30 shows the results of the Convex-Hull test over the 5x5 km² areas around the central coordinate of each sub-site. The strict and large convex-hulls are high around the test sites, greater than 60% for the five sub-sites. Even Meteopole (MTO) site presents more than 50%, a quite good result despite this area includes urban areas from Toulouse city (see Table 4).

Table 4: Percentages of convex-hull test over the study areas (5x5 km²) during the AHSPECT campaign on 22nd to 25th June, 2015 (South-West, France). Convex hull values: 0= extrapolation of TF, 1= strict convex hull and 2= large convex hull.

Field Campaign		Quality Flags (%)			
AHSPECT campaign		5x5 km ²			
SITE		0	1	2	1 & 2
Meteopole	MTO	40	54	6	60
Peyrousse	PEY	29	65	6	71
Urgons	URG	10	86	4	90
Creón d'Armagnac	CRE	30	66	4	70
Condom	CON	27	69	4	73
Savenes	SAV	32	64	4	68

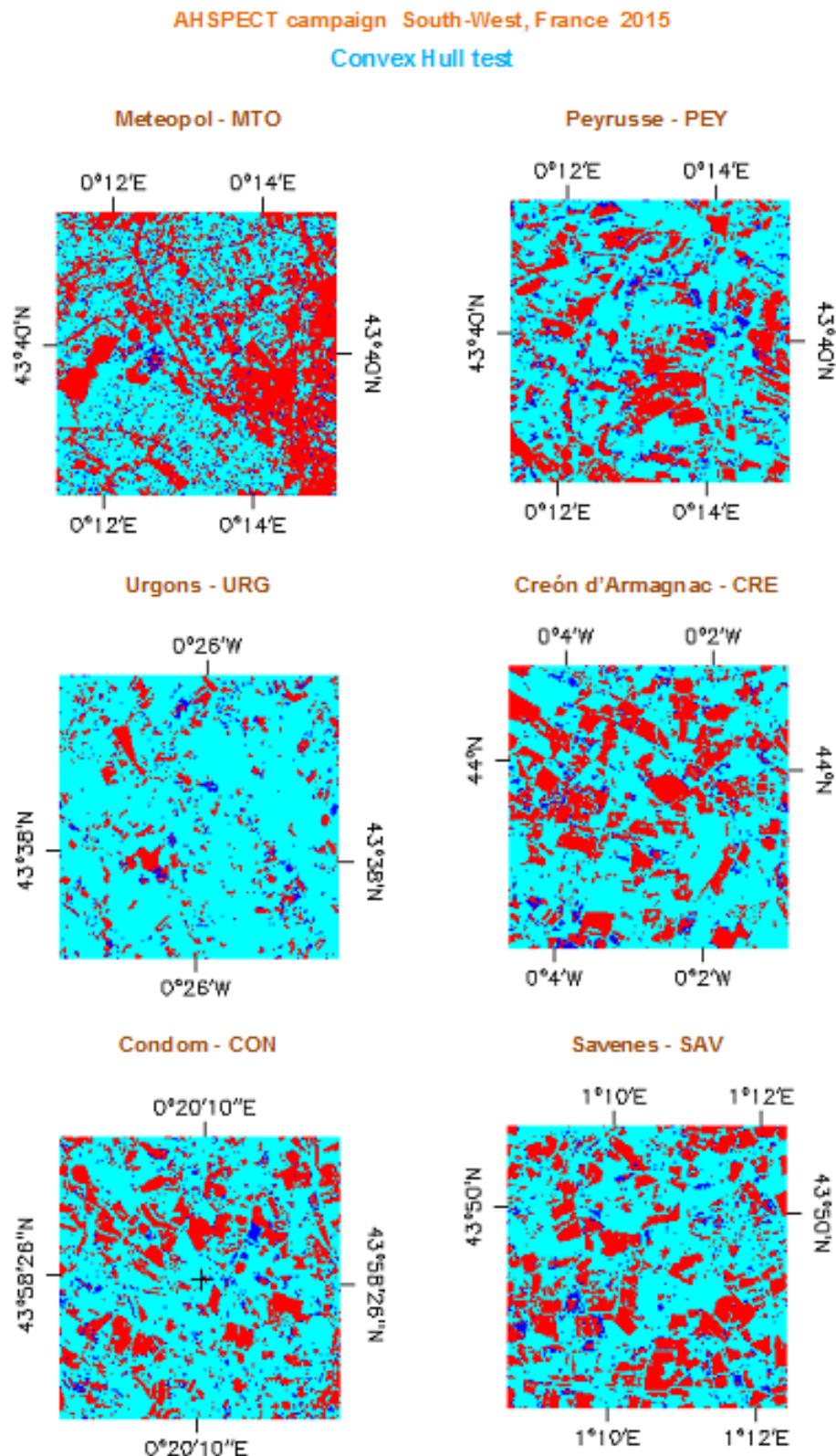


Figure 30: Convex Hull test over 5x5 km² areas: clear and dark blue correspond to the pixels belonging to the 'strict' and 'large' convex hulls. Red corresponds to the pixels for which the transfer function is extrapolating, during the AHSPECT campaign on 22nd to 25th June, 2015 (South-West, France).

6. PRODUCTION OF GROUND-BASED MAPS

6.1. IMAGERY

The Landsat-8 image was acquired the 23rd June, 2015 (see Table 5 for acquisition geometry). We selected 4 spectral bands in the VIS, NIR and SWIR regions ranging from 530 nm to 1650 nm with a nadir ground sampling distance of 30 m. For the transfer function, the input satellite product used is Top of Atmosphere (TOA) reflectance. The projection is UTM 31 North, WGS-84.

Table 5: Acquisition geometry of Landsat-8 data used for retrieving high resolution maps.

Landsat-8 METADATA	
Platform / Instrument	Landsat-8 / OLI_TIRS
Path	199
Row	30
Selected Bands	B3(green) : 0.53-0.59 μm B4(red) : 0.64-0.67 μm B5(NIR) : 0.85-0.88 μm B6(SWIR1) : 1.58-1.65 μm
AHSPECT campaign 22nd to 25th June, 2015	
Acquisition date	2015.06.23 10:41:45
Illumination Azimuth angle	133.985°
Illumination Elevation angle	64.335°
Ground control points verify	94
Geometric RMSE Verify	4.317

6.2. THE TRANSFER FUNCTION

6.2.1. The regression method

If the number of ESUs is enough, multiple robust regression 'REG' between ESUs reflectance and the considered biophysical variable can be applied (Martínez et al., 2009): we used the 'robustfit' function from the Matlab statistics toolbox. It uses an iteratively re-weighted least squares algorithm, with the weights at each iteration computed by applying the bi-square function to the residuals from the previous iteration. This algorithm provides lower weight to ESUs that do not fit well.

The results are less sensitive to outliers in the data as compared with ordinary least squares regression. At the end of the processing, two errors are computed: weighted RMSE (using the weights attributed to each ESU) (RW) and cross-validation RMSE (leave-one-out method) (RC).

As the method has limited extrapolation capacities, a flag image (Figure 29 and Figure 30), based on the convex hulls, is included in the final ground-based maps in order to inform the users on the reliability of the estimates.

Note that all the ground data points within the selected Landsat-8 images have been considered at the same time, rather than to apply one regression for each sub-site. This will increase considerably the number of ground references for having a more robust regression. This was also possible considering the similar landscape of all sub-sites (except the Sabres that was finally not included as it is not covered by the Landsat scene)

6.2.2. Band combination

Figure 31 shows the errors (RW, RC) obtained for the several band combinations using TOA reflectance. Since the large scene presents many senescent and harvested fields, we have selected the NDVI as input for the transfer function (exponential relationship with LAI_{eff} and LAI, and linear relationship with FAPAR and FCOVER, see section 6.2.3). Note that NDVI shows the lower errors for LAI_{eff} or LAI (for cross-validation RMSE), whereas NDVI shows similar errors than 4-bands combination for FAPAR and FCOVER, but NDVI assures good consistency of the transfer function maps over bare/senescent areas.

AHSPECT campaign South-West, France 2015

Test of regressions

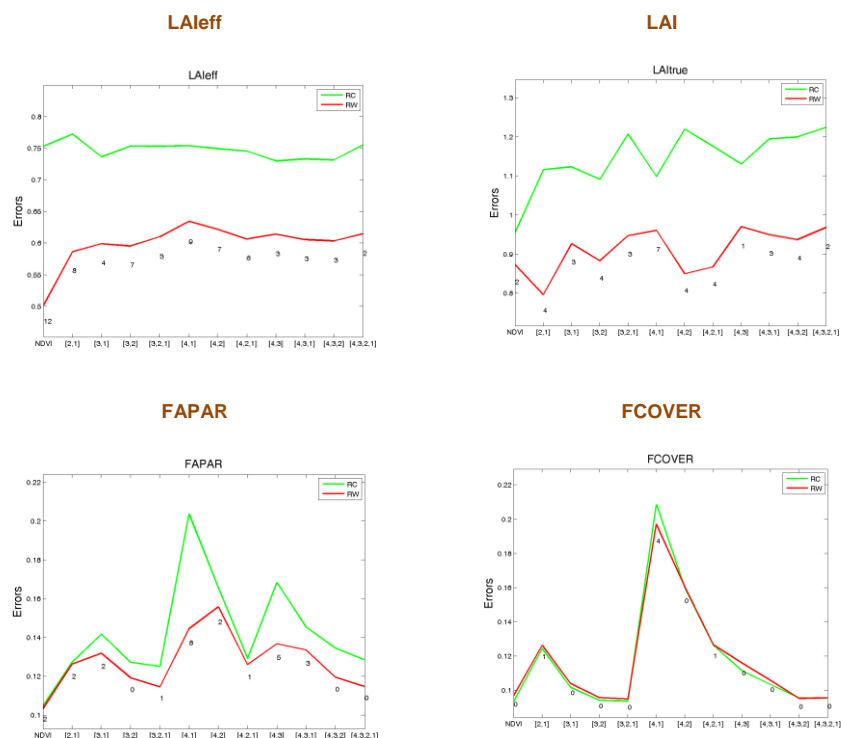


Figure 31: Test of multiple regression (TF) applied on different band combinations. Band combinations are given in abscissa (1=GREEN, 2=RED, 3=NIR and 4=SWIR). The weighted root mean square error (RMSE) is presented in red along with the cross-validation RMSE in green. The numbers indicate the number of data used for the robust regression with a weight lower than 0.7 that could be considered as outliers. AHSPECT campaign on 22nd to 25th June, 2015 (South-West, France).

6.2.3. The selected Transfer Function

The applied transfer function is detailed in Table 6, along with its weighted (RW) and cross-validated (RC) errors.

For the FAPAR and FCOVER, a simple linear relationship with NDVI was selected:

$$FAPAR = a + b \cdot NDVI \quad \text{Eq. (6)}$$

$$FCOVER = a + b \cdot NDVI \quad \text{Eq. (7)}$$

For the LAI_{eff} and LAI, an exponential relationship with NDVI was selected according to Baret et al., (1989):

$$LAI_{eff} = a + b \cdot \ln \left(\frac{NDVI_{\infty} - NDVI}{NDVI_{\infty} - NDVI_s} \right) \quad \text{Eq. (8)}$$

$$LAI = a + b \cdot \ln \left(\frac{NDVI_{\infty} - NDVI}{NDVI_{\infty} - NDVI_s} \right) \quad \text{Eq. (9)}$$

Where b represents the extinction coefficient which depends on the average leaf angle inclination, solar zenith angle and diffuse reflectance and transmittance of the leaves. “b” was set empirically with the ground data for each transfer function, as well as the residuals “a”. NDVI_s represents the typical NDVI of bare soil areas and NDVI_∞ represents the NDVI of fully developed canopies, both assumed to be constant over the image. NDVI_s was set to 0.12 and NDVI_∞ to 0.67 based on the histogram of the NDVI over the scene.

Table 6: Transfer function applied to the whole site for LAI_{eff}, LAI, instantaneous FAPAR at 10:00 SLT and FCOVER. RW stands for weighted RMSE, whereas RC stands for cross-validation RMSE.

Variable	Band Combination	RW	RC
AHSPECT campaign, South-West (France), June 2015			
LAI_{eff}	$0.075 - 1.312 \cdot \ln \left(\frac{0.67 - NDVI}{0.5} \right)$	0.50	0.73
LAI	$0.206 - 1.795 \cdot \ln \left(\frac{0.67 - NDVI}{0.5} \right)$	0.87	0.87
FAPAR	$- 0.209 + 1.783 \cdot NDVI$	0.10	0.11
FCOVER	$- 0.206 + 1.687 \cdot NDVI$	0.01	0.01

Figure 32 shows scatter-plots between ground observations and their corresponding transfer function (TF) estimates. A good correlation is observed for the LAI_{eff}, LAI, FAPAR and FCOVER with points distributed along the 1:1 line. Note that some underestimated points (TF values lower than ground data) were observed for ESUs #39 to #46 (sub-site CRE), corresponding to densest corn crops (height around 2m). The larger discrepancy (ESU#43)

is clearly associated to an outlier of the ground data (see Figure 26). For LAI, there are less ESUs under-estimated for this field as only DHP provides actual LAI estimates (see Table 2). The resulting TF maps are however not saturated, and LAI_{eff} values goes up to 4, and up to 6 for LAI. For low values, the TF tends to slightly overestimate the bare soils (LAI around 0.5, FAPAR and FCOVER ranging between 0.05 and 0.1). The largest deviations were found for wheat/harvested fields. This is a limitation of the accuracy of these empirical maps, as the NDVI of the senescent crops (yellow color) is slightly higher than for bare soils, this is particularly high for some control points (ESU#48 Harvested, ESU#55, Wheat) not used to compute the transfer function. There is some dispersion which should be partly attributed to uncertainties in the ground data and geo-locations errors.

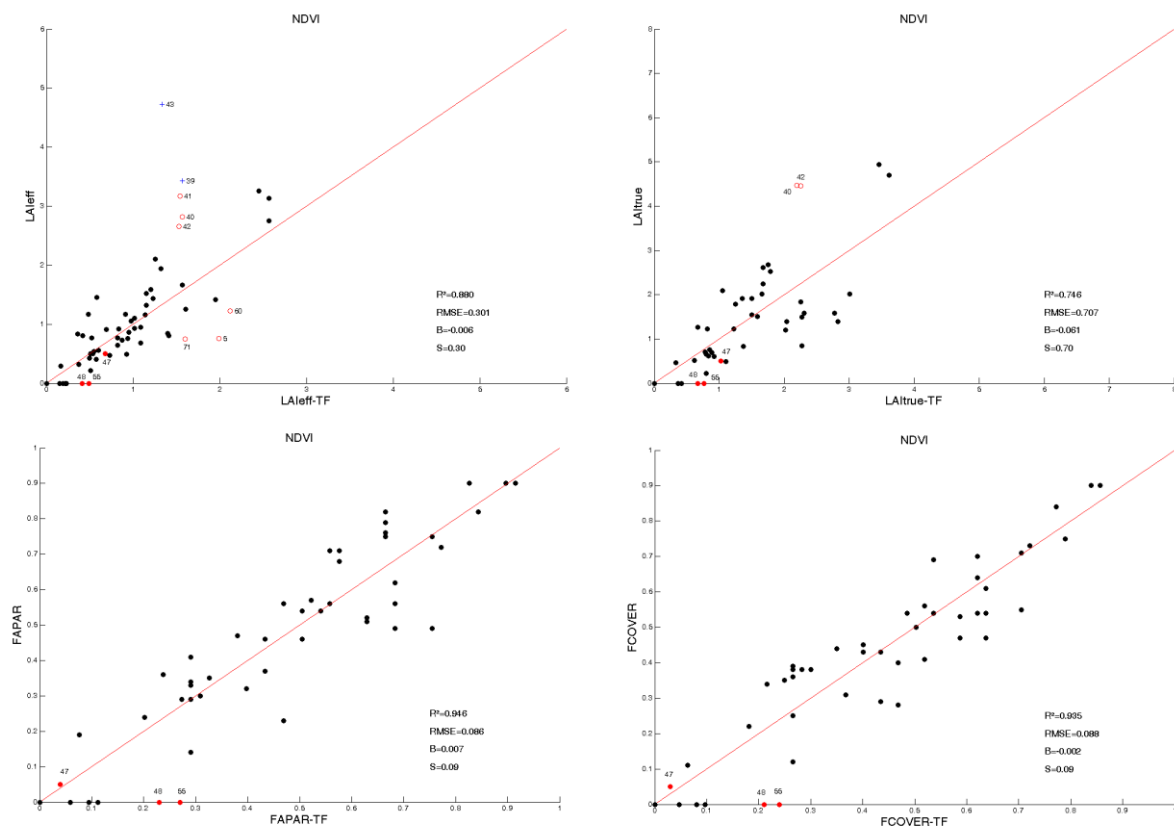


Figure 32: Scatter-plots of LAI_{eff}, LAI, FAPAR and FCOVER estimated values versus ground measurements. Full dots: Weight>0.7. Empty dots: 0<Weight<0.7. Crosses: Weight=0. AHSPECT campaign on 22nd to 25th June, 2015 (South-West, France). Numbers in the dots identifies the corresponding ESU. Red dots are control points not used in the empirical regression.

6.3. THE HIGH RESOLUTION GROUND BASED MAPS

The high resolution maps are obtained applying the selected transfer function (Table 6) to the Landsat-8 TOA reflectance. The study area (overlapping AHSPECT area with Landsat-8 199/30) has been extended to 76x160 km² (centre located at 43.6733N, 0.5617E, UTM zone

31 North, Datum WGS-84). Figure 33 to Figure 40 present the TF biophysical variables over the whole area and the 5x5 km² areas delivered for validation over each sub-site. Note the gradient of vegetation cover over the different sub-sites. Figure 29 and Figure 30 show the Quality Flag included in the final product.

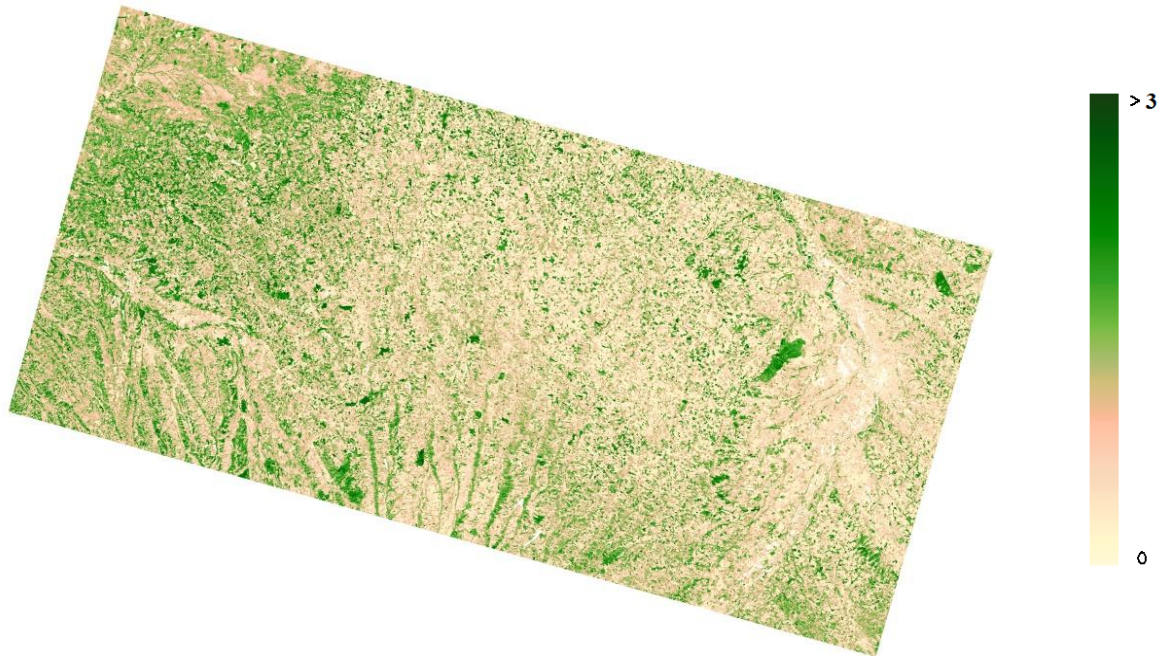


Figure 33: Ground-based LA_{eff} maps (76x160 km²) retrieved during the AHSPECT campaign on 22nd to 25th June, 2015 (South-West, France).

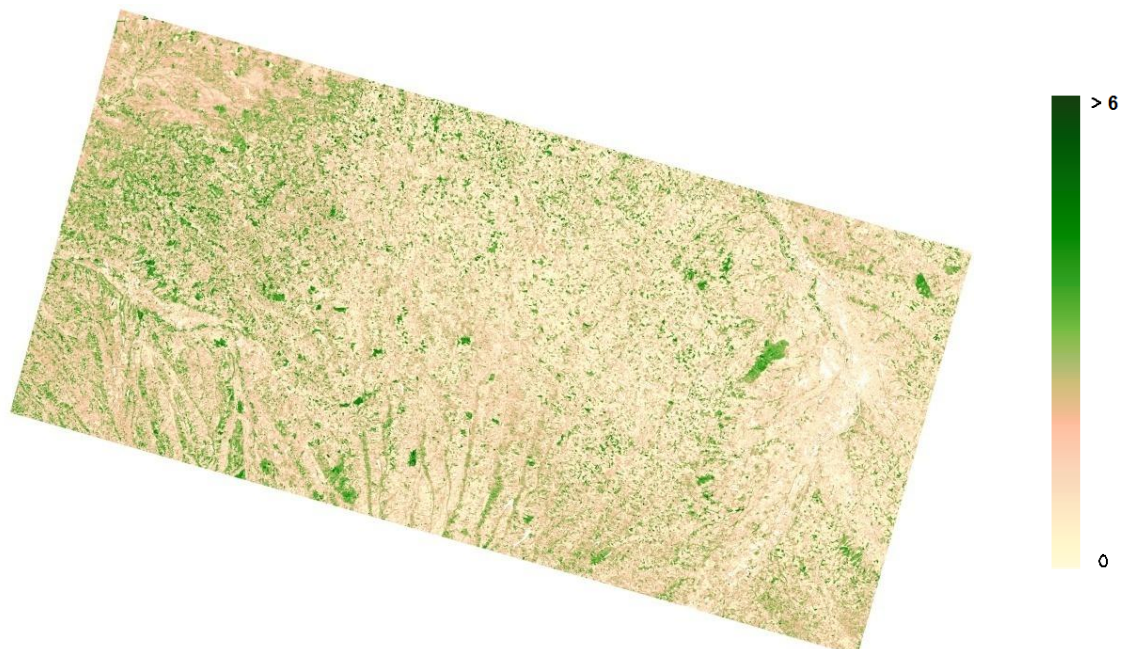


Figure 34: Ground-based LAI maps (76x160 km²) retrieved during the AHSPECT campaign on 22nd to 25th June, 2015 (South-West, France).

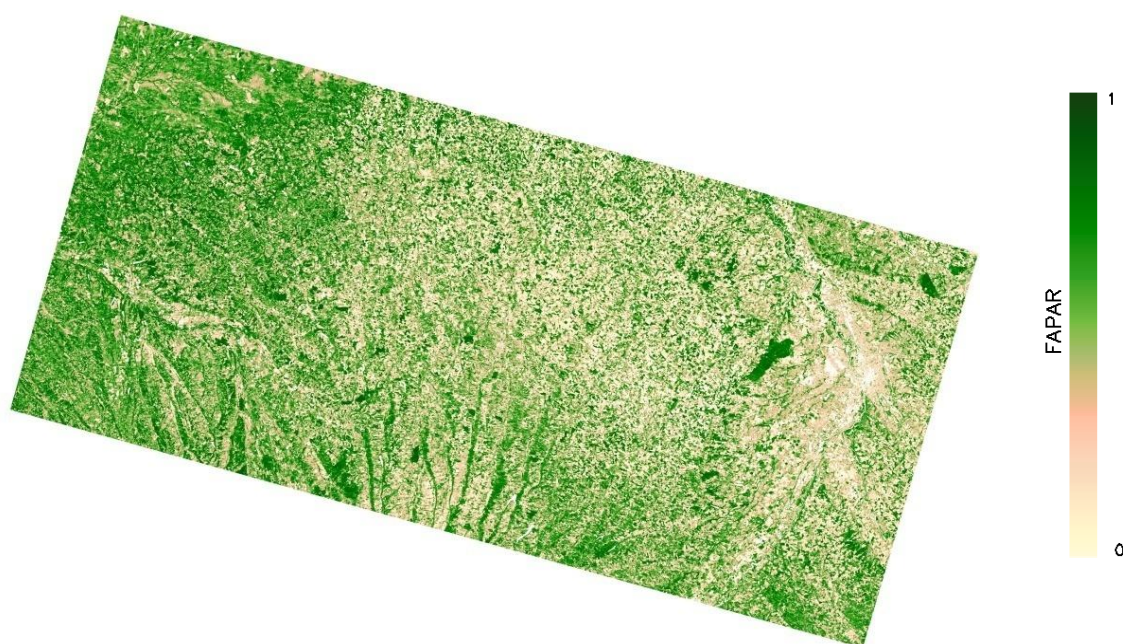


Figure 35: Ground-based FAPAR maps (76x160 km²) retrieved during the AHSPECT campaign on 22nd to 25th June, 2015 (South-West, France).

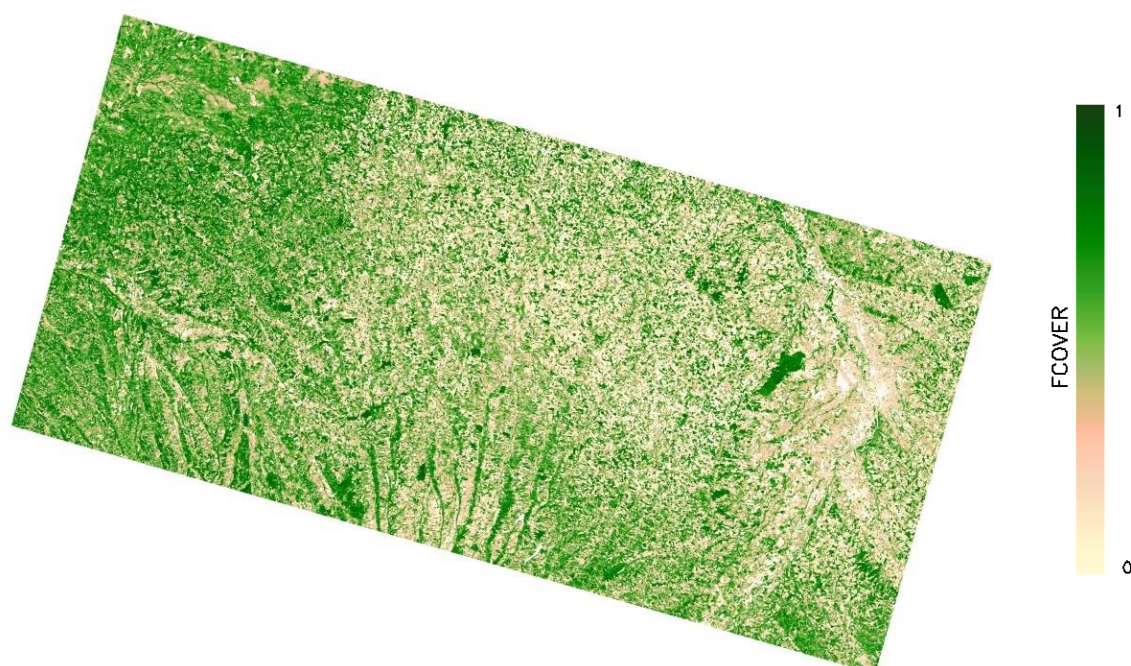


Figure 36: Ground-based FCOVER maps (76x160 km²) retrieved during the AHSPECT campaign on 22nd to 25th June, 2015 (South-West, France).

AHSPECT campaign South-West, France 2015

LAleff

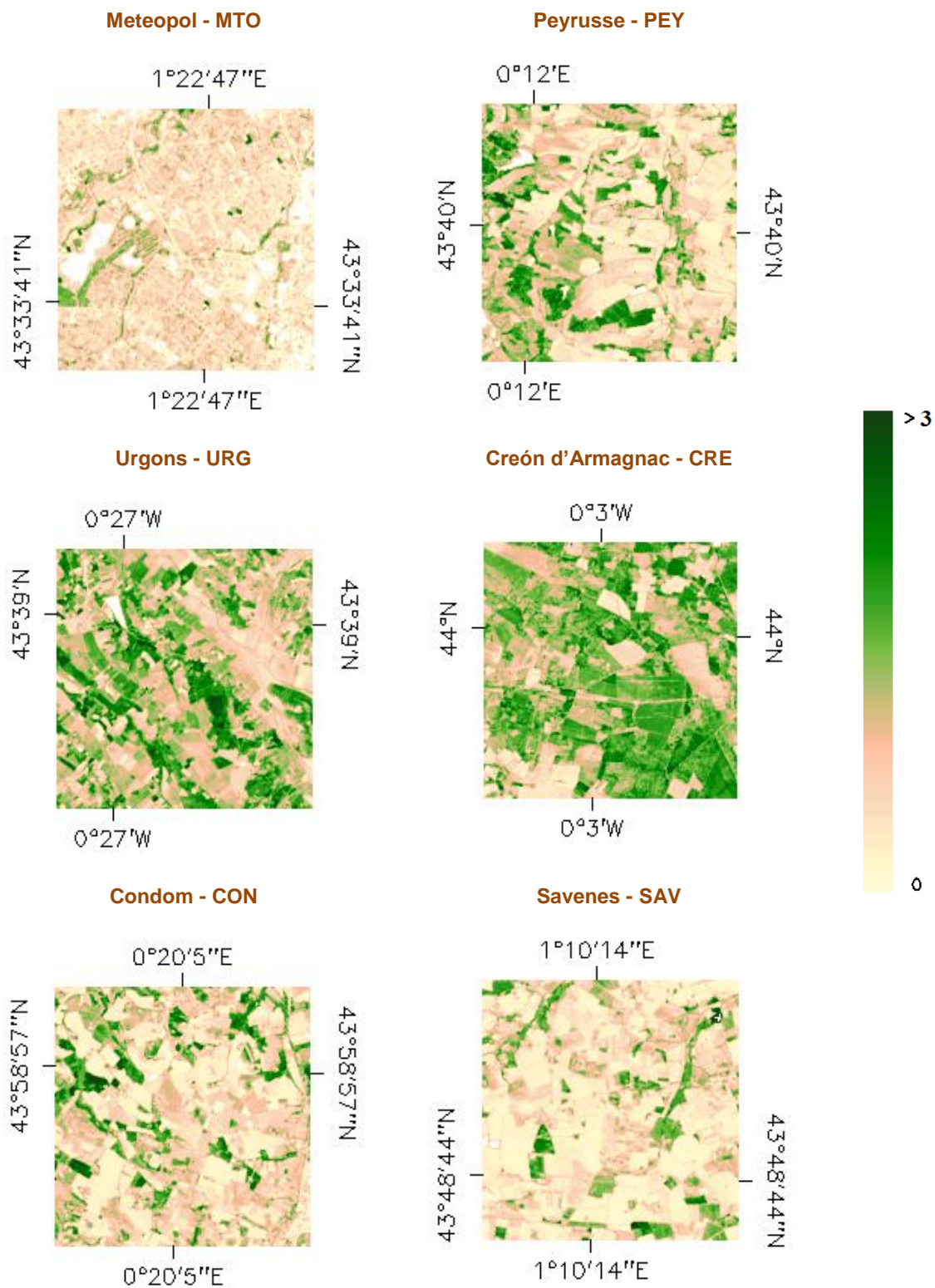


Figure 37: Ground-based LAleff maps (5x5 km²) retrieved during the AHSPECT campaign on 22nd to 25th June, 2015 (South-West, France).

AHSPECT campaign South-West, France 2015

LAI

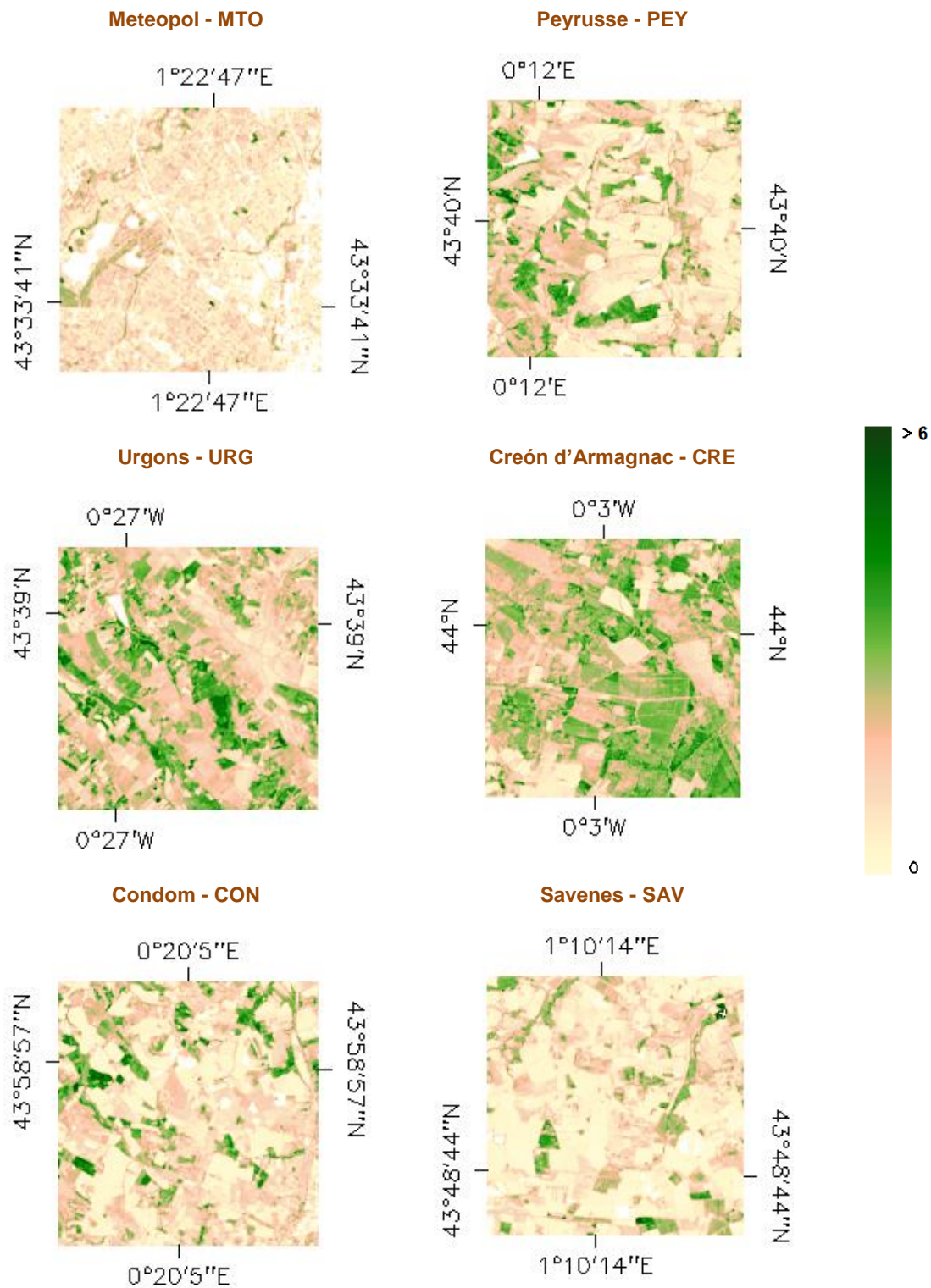


Figure 38: Ground-based LAI maps (5x5 km²) retrieved during the AHSPECT campaign on 22nd to 25th June, 2015 (South-West, France).

AHSPECT campaign South-West, France 2015

FAPAR

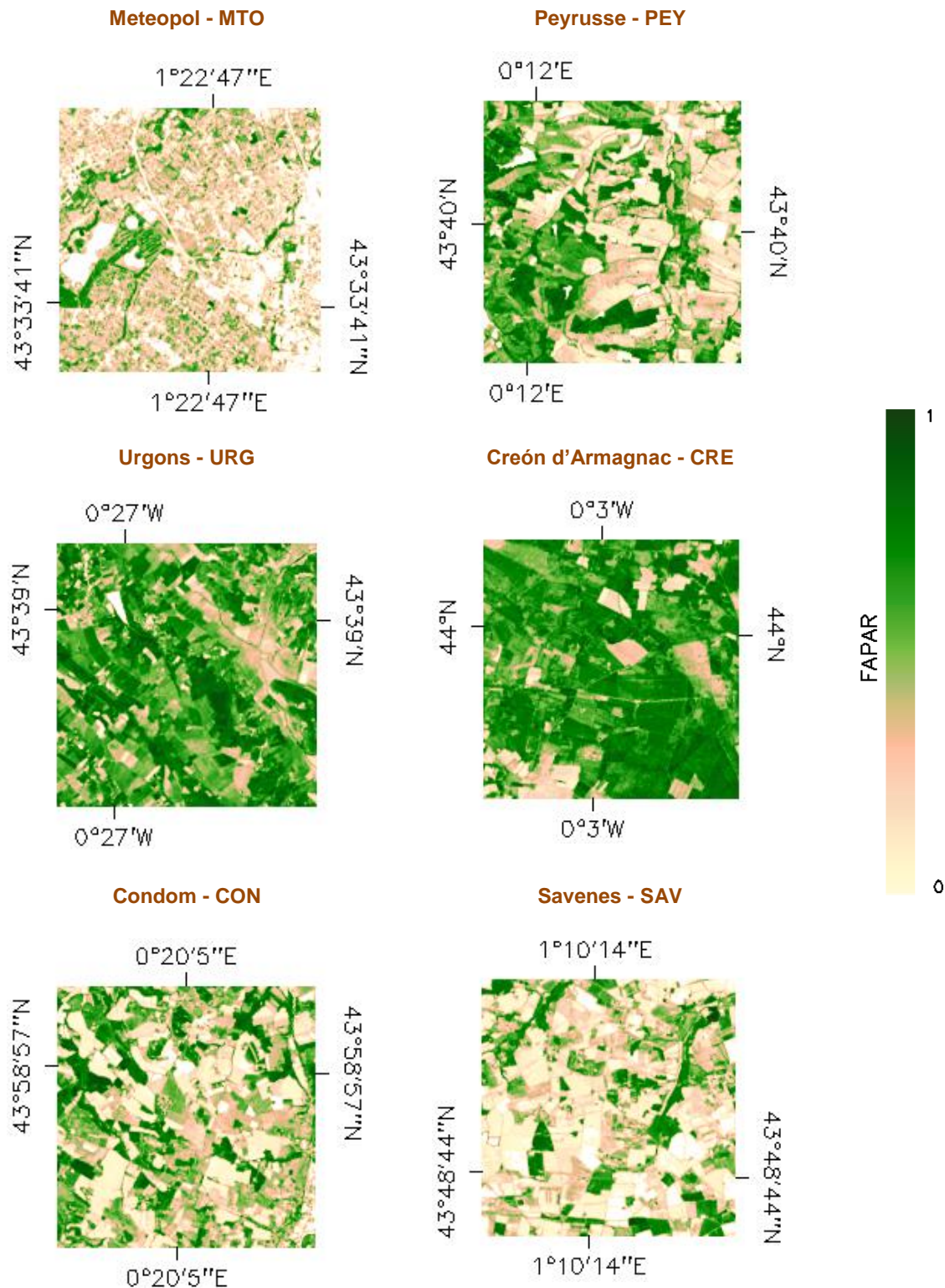


Figure 39: Ground-based FAPAR at 10:00 SLT maps (5x5 km²) retrieved during the AHSPECT campaign on 22nd to 25th June, 2015 (South-West, France).

AHSPECT campaign South-West, France 2015

FCOVER

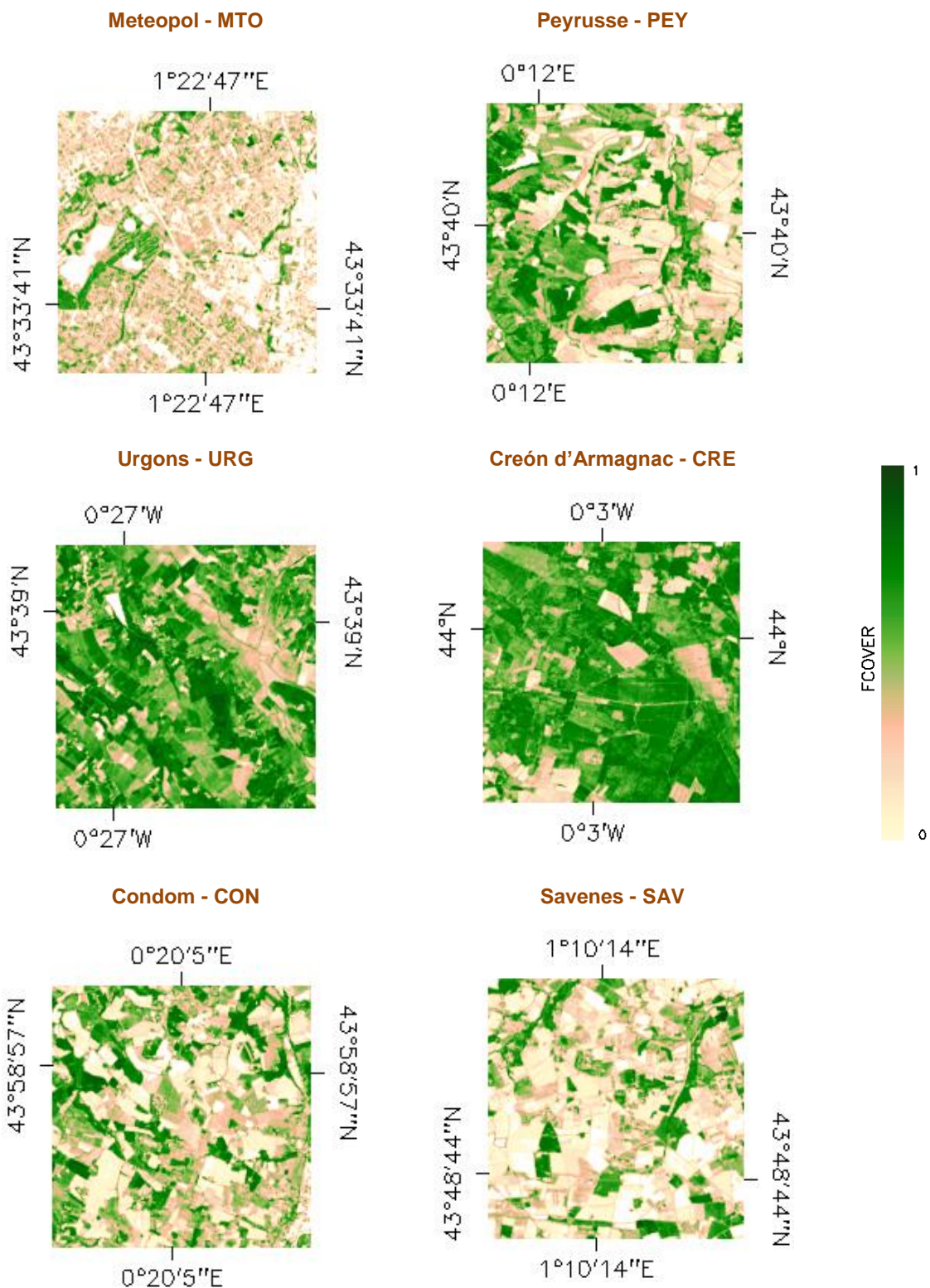


Figure 40: Ground-based FCOVER map (5x5 km²) retrieved during the AHSPECT campaign on 22nd to 25th June, 2015 (South-West, France).

These 5x5 km² maps are provided for validation of satellite products at different resolutions. Mean values over 3x3 km² are provided in Table 7.

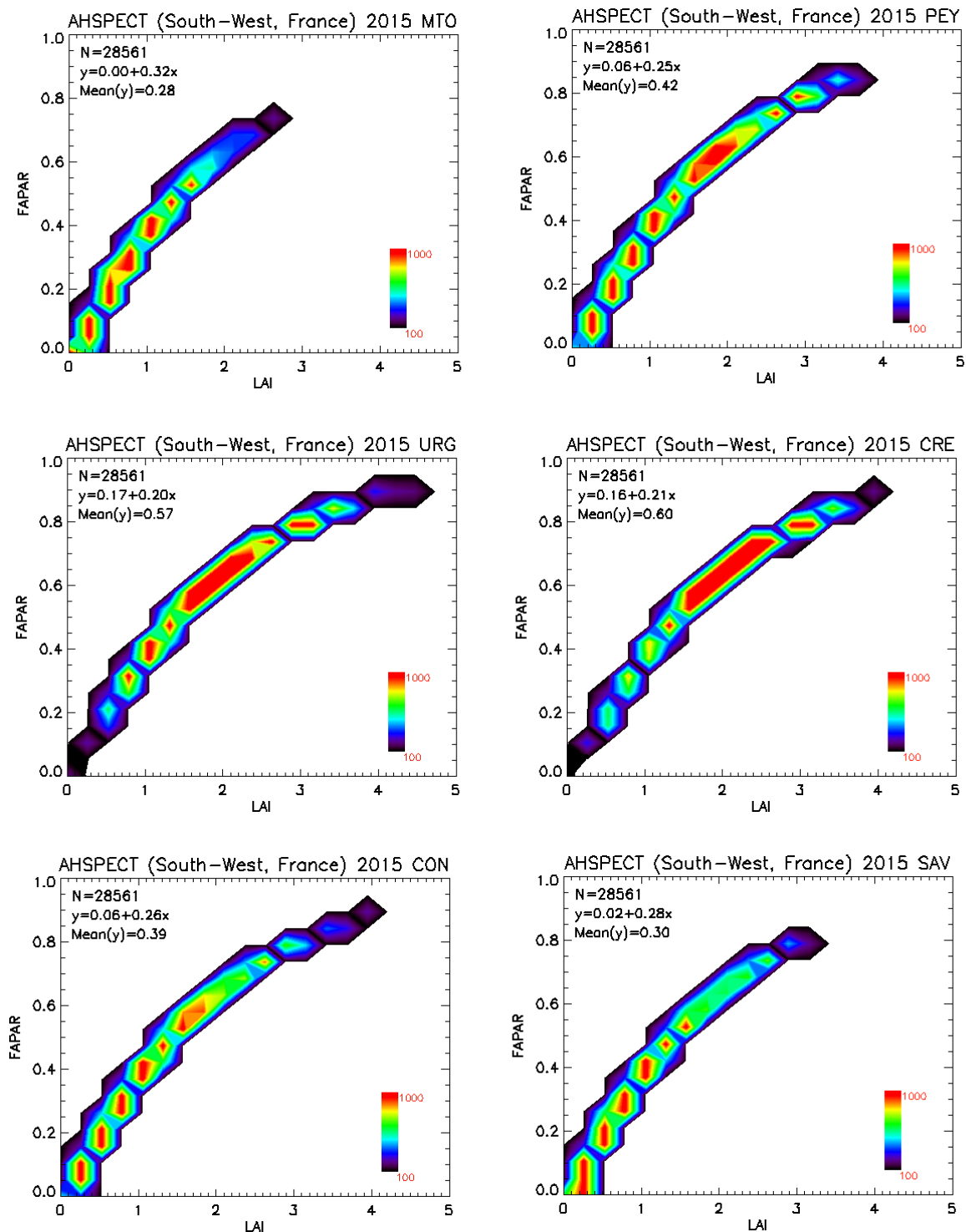


Figure 41: Scatter-plots LAI vs FAPAR ground-based maps over the AHSPECT sub-sites, 22nd to 25th June, 2015 (South-West, France).

Scatters-plots (Figure 41 and Figure 42) between biophysical variables show the good consistency of the 5x5 km² ground-based maps (all pixels), showing the expected exponential (LAI vs FAPAR) and linear (FAPAR vs FCOVER) trends observed with the ground data. Note that FAPAR provides slightly higher values than FCOVER as expected (slope higher than 1).

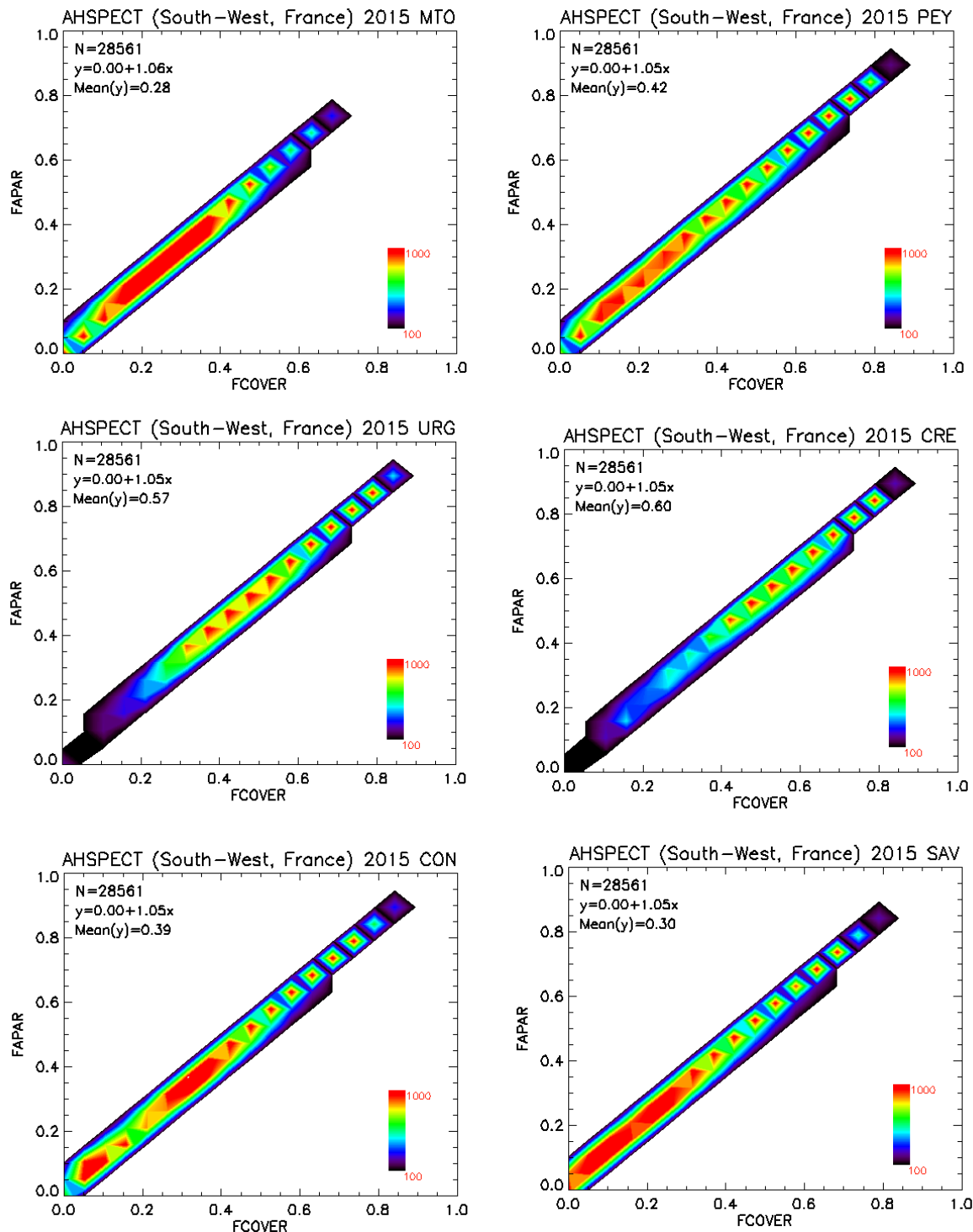


Figure 42: Scatter-plots FAPAR vs FCOVER ground-based maps over the AHSPECT sub-sites, 22nd to 25th June, 2015 (South-West, France).

6.3.1. Mean Values

Mean values of a 3x3 km² area centered in the test site are provided for the validation of 1 km satellite products in agreement with the CEOS OLIVE direct dataset (Table 7). For the validation of coarser resolutions product (e.g. LSA SAF SEVIRI products) a larger area should be considered. For this reason, ground based maps are provided at 5x5 km².

Table 7: Mean values and standard deviation (STD) of the HR biophysical maps for the selected 3 x 3 km² areas during the AHSPECT campaign on 22nd to 25th June, 2015 (South-West, France).

AHSPECT campaign											
3x3 km ²		LATITUDE	LONGITUDE	Mean Values				STDV Values			
				LAI _{eff}	LAI	FAPAR	FCOVER	LAI _{eff}	LAI	FAPAR	FCOVER
Meteopol	MTO	43.572812° N	+1.374512° E	0.55	0.85	0.28	0.26	0.37	0.51	0.17	0.16
Peyrousse	PEY	43.666229° N	+0.219540° E	0.90	1.33	0.41	0.38	0.60	0.83	0.22	0.21
Urgons	URG	43.639704° N	-0.433956° E	1.39	2.01	0.60	0.55	0.61	0.84	0.17	0.16
Creón d'Armagnac	CRE	43.993601° N	-0.046897° E	1.51	2.17	0.63	0.59	0.49	0.67	0.14	0.13
Condom	CON	43.974290° N	+0.335969° E	0.77	1.16	0.36	0.33	0.59	0.80	0.22	0.21
Savenes	SAV	43.824221° N	+1.174945° E	0.65	0.99	0.31	0.29	0.51	0.70	0.21	0.20

Table 8 describes the content of the geo-biophysical maps in the "BIO_YYYYMMDD_LANDSAT8_site_sub-site ETF_area" files.

Nomenclature: BIO_YYYYMMDD_SENSOR_Site ETF_Area

where: BIO stands for Biophysical (LAI_{eff}, LAI, FAPAR and FCOVER)

SENSOR = LANDSAT8

YYYYMMDD = Campaign date

Site = SouthWest_SUB-SITE (MTO, PEY, URG, CRE, CON and SAV)

ETF stands for Empirical Transfer Function

Area = 5x5

Table 8: Content of the dataset.

Parameter	Dataset name	Range	Variable Type	Scale Factor	No Value
LAI effective	LAI _{eff}	[0, 7]	Integer	1000	-1
LAI	LAI	[0, 7]	Integer	1000	-1
FAPAR 10:00 SLT	FAPAR	[0, 1]	Integer	10000	-1
Fraction of Vegetation Cover	FCOVER	[0, 1]	Integer	10000	-1
Quality Flag	QFlag	0,1,2 (*)	Integer	N/A	-1

(*) 0 means extrapolated value (low confidence), 1 strict interpolator (best confidence), 2 large interpolator (medium confidence).

7. CONCLUSIONS

The FP7 ImagineS project continues the innovation and development activities to support the operations of the Copernicus Global Land service. This report summarizes the field campaign and vegetation ground measurements collected by EOLAB during the first phase of the EUFAR AHSPECT airborne campaign, carried out during the 22nd to 25th of June, 2015, over the South-West region of France (from Toulouse to the Atlantic coast).

Firstly, this report presents the ground data collected over a number of sub-sites. A total of 73 ESUs were characterized with digital hemispherical photos (DHP), ceptometer AccuPAR, and LICOR LAI-2200 PCA, over a total of 32 fields and 7 sub-sites (i.e., Meteopole, Peyrousse, Urgons, Sabres, Creón d'Armagnac, Condom and Savenès). Most of the ESUs correspond to corn crops, but in different growing states. Sunflower, soybean, pine plantation, wheat and grasslands canopies were also sampled. The sampling protocol was in agreement with ImagineS guidelines for field campaign and previous validation experiments (e.g. VALERI). The ground data was mainly collected with DHP and processed with CAN-EYE. A quality check of the results was performed, identifying problematic ESUs that were reprocessed when needed. Unreliable clumping indices for some canopies were identified in the database. A consistent and reliable ground data set was finally provided in an excel file with all the ground data information collected during the campaign.

Secondly, high resolution ground-based maps of the biophysical variables have been produced over the site. Ground-based maps have been derived using high resolution imagery (Landsat-8 TOA Reflectance) according with the CEOS LPV recommendations for validation of low resolution satellite sensors. Transfer functions have been derived by multiple robust regressions between ESUs reflectance and the several biophysical variables. Because the scene presents many senescent and harvested fields, we have selected the NDVI as input for the transfer function (exponential relationship with LAI_{eff} and LAI, and linear relationship with FAPAR and FCOVER). NDVI assures good consistency of the maps over the whole area, but also provides low RMSE errors. The weighted RMSE values for the several transfer function estimates are 0.30 for LAI_{eff}, 0.71 for LAI, and 0.09 for instantaneous FAPAR at 10:00 SLT and for FCOVER. Nevertheless, a positive bias is observed for senescent wheat fields or harvested fields, which is a limitation of the method.

The quality flag map based on the convex-hull analysis shows quite good quality (greater than 60% at 5x5 km² sub-sites). The sub-sites maps over a 5x5 km² area are provided.

The biophysical variable maps over six sub-sites (Sabres was not covered by the Landsat8 scene 199/30 used for up-scaling) are available in geographic (UTM 31 North projection WGS-84) coordinates at 30 m resolution. Mean values and standard deviation for LAI_{eff}, LAI, FCOVER and FAPAR were computed over an area of 3x3 km² for validation of low and medium resolution satellite products. These maps generated over AHSPECT sites are very valuable for the validation of satellite products, and demonstrates the value of multi-sites field campaigns performing transects along a region of interest.

8. ACKNOWLEDGEMENTS

This work is supported by the FP7 IMAGINES project under Grant Agreement N°311766. Landsat-8 HR imagery is provided through the USGS Global Visualization service. The field campaign was partly funded by EUFAR. Special thanks are given to Jean-Louis Roujean (Meteo-France) for the coordination (and local support) of the AHSPECT campaign.

9. REFERENCES

Baret, F., G. Guyot and Major, D. (1989). Crop biomass evaluation using radiometric measurements. *Photogrammetria* 43:241-256.

Baret, F and Fernandes, R. (2012). Validation Concept. VALSE2-PR-014-INRA, 42 pp.

Camacho, F., Baret, F., and Lacaze R. (2015). Guidelines for a Field campaign. (Available at ImagineS website: <http://fp7-imagines.eu/pages/documents.php>).

Camacho, F., Cernicharo, J., Lacaze, R., Baret, F., and Weiss, M. (2013). GEOV1: LAI, FAPAR Essential Climate Variables and FCOVER global time series capitalizing over existing products. Part 2: Validation and intercomparison with reference products. *Remote Sensing of Environment*, 137: 310-329.

Decagon Devices, Inc. (2014). AccuPAR PAR/LAI Ceptometer. Model LP80 manual. <http://www.decagon.com>

Demarez, V., Duthoit, S., Baret, F., Weiss, M. and Dedieu, G. (2008). Estimation of leaf area and clumping indexes of crops with hemispherical photographs. *Agricultural and Forest Meteorology*, 148, 644-655.

Fernandes, R., Plummer, S., Nightingale, J., et al. (2014). Global Leaf Area Index Product Validation Good Practices. CEOS Working Group on Calibration and Validation - Land Product Validation Sub-Group. *Version 2.0: Public version made available on LPV website*.

Martínez, B., García-Haro, F. J., & Camacho, F. (2009). Derivation of high-resolution leaf area index maps in support of validation activities: Application to the cropland Barrax site. *Agricultural and Forest Meteorology*, 149, 130–145.

Miller, J.B. (1967). A formula for average foliage density. *Aust. J. Bot.*, 15:141-144

Morisette, J. T., Baret, F., Privette, J. L., Myneni, R. B., Nickeson, J. E., Garrigues, S., et al. (2006). Validation of global moderate-resolution LAI products: A framework proposed within the CEOS land product validation subgroup. *IEEE Transactions on Geoscience and Remote Sensing*, 44, 1804–1817.

Latorre, C., Camacho, F., Pérez, M., Beget M.E. and Di Bella, C. (2014). “Vegetation Field Data and Production of Ground-Based Maps: 25 de Mayo site. La Pampa, Argentina” report. 18 -20 (Available at ImagineS website: <http://fp7-imagines.eu/pages/documents.php>).

LI-COR Inc., Lincoln, Nebraska, (2013). [http://envsupport.licor.com/docs/LAI-2200C Instruction Manual.pdf](http://envsupport.licor.com/docs/LAI-2200C%20Instruction%20Manual.pdf)

Weiss, M., Baret, F., Smith, G.J., Jonckheere, I. and Coppin, P., (2004). Review of methods for in situ leaf area index (LAI) determination. Part II. Estimation of LAI, errors and sampling. *Agricultural and Forest Meteorology*. 121, 37–53.

Weiss M. and Baret F. (2010). CAN-EYE V6.1 User Manual

Welles, J.M. and Norman, J.M., 1991. Instrument for indirect measurement of canopy architecture. *Agronomy J.*, 83(5): 818-825.

10. ANNEX I: DESCRIPTION OF ESUS

Table 9: Total of ESUs collected during the AHSPECT campaign on 22nd to 25th June, 2015 (South-West, France). Cardinality of fields, plot label, cardinality of ESUs, label, latitude, longitude, device, land cover type and date.

Location	ESU #	Label	Northing Coord	Easting Coord	Instrumentation	Land Cover	Date (dd/mm/yyyy)	
Meteopol (MTO)	1	MTO_G1	43.5738	1.3750	DHP	Grass	22/06/2015	
	2	MTO_G2	43.5734	1.3748	DHP			
Peyrouse (PEY)	3	PEY_W11	43.6672	0.2205	DHP	Wheat	23/06/2015	
	4	PEY_SF11	43.6699	0.2197	DHP	SunFlower		
	5	PEY_SF12	43.6695	0.2132	DHP			
	6	PEY_SF13	43.6703	0.2190	DHP			
	7	PEY_SF14	43.6700	0.2186	DHP			
	8	PEY_SF15	43.6696	0.2177	DHP			
	9	PEY_W21	43.6671	0.2236	DHP	Wheat		
	10	PEY_SF21	43.6590	0.2390	DHP	SunFlower		
	11	PEY_SF22	43.6590	0.2400	DHP			
	12	PEY_SF23	43.6588	0.2412	DHP	Wheat		
	13	PEY_W31	43.6582	0.2400	DHP			
	14	PEY_SF31	43.6591	0.2371	DHP	SunFlower		
	Urgons (URG)	15	URG_C11	43.6392	-0.4356	DHP		Corn
		16	URG_C12	43.6389	-0.4352	DHP		
17		URG_C21	43.6405	-0.4350	LAI-2200			
18		URG_C22	43.6406	-0.4352	DHP			
19		URG_C23	43.6409	-0.4346	LAI-2200			
20		URG_C24	43.6411	-0.4347	DHP			
21		URG_C31	43.6391	-0.4419	LAI-2200			
22		URG_C32	43.6393	-0.4421	DHP			
23		URG_C33	43.6398	-0.4422	LAI-2200			
24		URG_C34	43.6391	-0.4423	DHP			
25		URG_C41	43.6387	-0.4408	LAI-2200			
26		URG_C42	43.6389	-0.4402	DHP			
Sabres (SAB)		27	SAB_C11	44.1474	-0.8447	LP80	24/06/2015	
		28	SAB_C12	44.1470	-0.8444	LAI-2200		
	29	SAB_C13	44.1473	-0.8439	DHP			
	29	SAB_C13	44.1473	-0.8439	LP80			
	30	SAB_C14	44.1476	-0.8435	LAI-2200			
	31	SAB_C15	44.1479	-0.8434	LP80			
	32	SAB_C16	44.1484	-0.8432	LAI-2200			
	33	SAB_C21	44.1466	-0.8451	DHP			
	34	SAB_C22	44.1457	-0.8445	DHP			
	35	SAB_PF11	44.1264	-0.8327	LAI-2200			
	35	SAB_PF11	44.1264	-0.8327	LP80			
	36	SAB_PF12	44.1265	-0.8325	DHP			
	36	SAB_PF12	44.1265	-0.8325	LAI-2200			
	36	SAB_PF12	44.1265	-0.8325	LP80			
37	SAB_PF13	44.1261	-0.8330	DHP				
38	SAB_PF14	44.1264	-0.8327	DHP				
Cre�n d'Armagnac (CRE)	39	CRE_C11	43.9938	-0.0465	LP80	25/06/2015		
	40	CRE_C12	43.9937	-0.0463	DHP			
	41	CRE_C13	43.9938	-0.0460	LAI-2200			
	42	CRE_C14	43.9940	-0.0460	DHP			
	43	CRE_C21	43.9928	-0.0461	LAI-2200			
	44	CRE_C22	43.9928	-0.0458	DHP			
	45	CRE_C23	43.9927	-0.0452	LAI-2200			
	46	CRE_C24	43.9927	-0.0452	DHP			
	47	CRE_G11	43.9938	-0.0440	visual inspection			
	48	CRE_H11	43.9971	-0.0370	visual inspection		Harvested	
	49	CRE_C31	43.9875	-0.0541	LAI-2200		Corn	
	50	CRE_C32	43.9876	-0.05375	DHP			
	51	CRE_C33	43.9876	-0.0533	DHP			
	52	CRE_C33	43.9874	-0.0532	LAI-2200			
Condom (CON)	53	CON_G11	43.9740	0.3378	DHP	Grass		
	54	CON_P11	43.9737	0.3363	DHP	Prunus Popplar		
	55	CON_W11	43.9737	0.3363	DHP	Wheat		
	56	CON_P21	43.9739	0.3345	DHP	Prunus Popplar		
	57	CON_P31	43.9757	0.3351	DHP	SunFlower		
	58	CON_SF11	43.9739	0.3405	DHP			
	59	CON_SF12	43.9746	0.3402	DHP			
	60	CON_SF13	43.9749	0.3396	DHP			
Saven�s (SAV)	61	SAV_W11	43.8243	1.1745	visual inspection	Wheat		
	62	SAV_H11	43.8235	1.1753	DHP	Harvested		
	63	SAV_SB11	43.8220	1.1736	DHP	SoyBean		
	64	SAV_SB12	43.8217	1.1735	LAI-2200			
	65	SAV_SB13	43.8213	1.1736	DHP			
	66	SAV_SB14	43.8210	1.1737	LAI-2200			
	67	SAV_SB21	43.8194	1.1739	LAI-2200			
	68	SAV_SB22	43.8191	1.1740	DHP	Wheat		
	69	SAV_W21	43.8198	1.1727	DHP			
	70	SAV_W31	43.8211	1.1730	DHP			
	71	SAV_SF12	43.8290	1.1773	DHP	SunFlower		
	72	SAV_SF13	43.8294	1.1773	DHP			
	73	SAV_SF14	43.8299	1.1772	DHP			